# One-dimensional Front Tracking Based on High Resolution Wave Propagation Methods

R. J. LeVeque[1] and K. M. Shyue[2]

**Abstract.** We present a simple approach to shock tracking in conjunction with conservative high resolution shock-capturing methods in one space dimension. An underlying uniform grid is used with additional grid interfaces introduced at appropriate points for tracked shocks. Conservative high resolution methods based on the large time step wave propagation approach are used on the resulting nonuniform grid. This method is stable even if some of the small cells created by the tracked interface are orders of magnitude smaller than the regular cells used to determine the time step. A fractional step method is used to handle source terms. Several calculations are presented to demonstrate the effectiveness of the method, including an unstable detonation wave calculation where mesh refinement in the reaction zone is required in addition to shock tracking. Stability and accuracy results of the method are also shown for some sample problems. The basic ideas described here can be extended to two space dimensions, as will be discussed in a sequel paper.

**Key words.** front tracking, shock tracking, finite volume methods, high resolution methods, conservation laws.

**AMS (MOS) subject classifications.** 65M06, 65M50, 76L05, 76M20.

**Running title:** Front tracking based on wave propagation.

**1. Introduction.** Our goal is to present a simple one-dimensional shock-tracking algorithm for nonlinear systems of conservation laws possibly including source terms,

$$u_t + f(u)_x = \psi(u). \tag{1.1}$$

We consider a system of $m$ equations, so $u \in \mathbb{R}^m$. The homogeneous system $u_t + f(u)_x = 0$ is assumed to be hyperbolic, in the sense that the flux Jacobian matrix $f'(u)$ is assumed to have real eigenvalues for each physically relevant value of the state variables $u$. This is true, for example, for the Euler equations of gas dynamics which we use as our model system. (See Section 5.) Source terms can arise in various ways. Geometric source terms arise when multi-dimensional gas dynamics is reduced to a one-dimensional problem using symmetry (e.g., radially symmetric flow) or by assuming that the cross-sectional flow is homogeneous, as in the quasi one-dimensional nozzle problem. Source terms that are more difficult to handle arise in the study of nonequilibrium or chemically reacting flows, for example in combustion problems. A model system of this form is solved in Section 8.

Clearly one-dimensional problems are of limited interest. However, there are some problems of sufficient interest and difficulty that shock tracking is worthwhile, particularly since it is relatively easy to implement in one space dimension and can provide a very clear picture of the wave pattern. A number of such algorithms have been proposed in the past (see Section 2). We believe that our approach is particularly simple and avoids some of the

[1] Departments of Mathematics and Applied Mathematics, University of Washington, Seattle, WA 98195.
[2] Department of Applied Mathematics and Statistics, SUNY at Stony Brook, Stony Brook, NY 11794.
To appear in SIAM J. Sci. Comput. Version of January 7, 1994.

difficulties encountered with other algorithms. The approach we pursue was first proposed in [20] for use in conjunction with the first order accurate Godunov method.

Many of the ideas presented here can also be extended to define a relatively simple multi-dimensional front tracking algorithm. A two-dimensional code based on the same approach has also been developed and used to solve a variety of problems, including shock propagation, the tracking of unstable interfaces in Rayleigh-Taylor and Kelvin-Helmholtz instabilities, and the solution of miscible and immiscible flow problems in porous media flow[36]. The two-dimensional algorithm will be presented in a sequel paper. The present paper presents many of the basic ideas necessary to understand the two-dimensional algorithm.

The basic idea of our shock tracking algorithm is quite simple. We use a high resolution finite volume method on a grid that varies from one time step to the next. The vast majority of grid cells do not vary. We have a fixed, uniform, underlying grid that is sufficient to represent the solution in smooth regions (although adaptive mesh refinement is also used for some problems, for example in the thin combustion region of the detonation problem considered in Section 8). Additional cell boundaries are introduced at the locations of discontinuities in the flow field, subdividing some regular cells into two or more subcells.

In a finite volume representation, the value in each grid cell represents the average value of the solution over that grid cell. By having a cell boundary at the discontinuity, we avoid the smearing and loss of accuracy that is inevitable when the discontinuity falls within a grid cell and the discrete solution must be averaged over the cell. By using a fully conservative high resolution shock capturing method, we ensure that features not being tracked are still accurately computed.

The high resolution methods we employ are based on solving Riemann problems at each interface, coupled with propagation of the resulting elementary waves. This Riemann solution gives, in particular, information about the propagation speed of tracked discontinuities. This information is used to choose the grid at the next time step in such a way that discontinuities remain sharp. Once the new grid has been chosen, the high resolution method we use takes essentially the same form on both regular and irregular cells.

An apparent difficulty with this approach is the fact that the discontinuity may fall arbitrarily close to a cell boundary of the underlying grid. Subdividing the cell can thus result in the creation of arbitrarily small grid cells. Since the finite volume method we employ is explicit, this can lead to either instability or a severe time step restriction. Most shock tracking methods face this difficulty, and it is often dealt with by adjusting or eliminating other cell boundaries to maintain a lower bound on the cell size. This leads to unnecessary complication of the algorithm.

We avoid this difficulty by using the "large time step" ideas developed by LeVeque [19],[21]. A high resolution method based on wave propagation is developed that remains stable in the presence of arbitrarily small cells, as described in Section 3. The main idea is that waves arising from the solution of Riemann problems at the cell boundaries are propagated the appropriate distance determined by the wave speed and time step, and used to update cell averages in any grid cell they pass through or enter. The wave may affect more than one cell if the neighboring cell is very small. In this manner the stencil of the method adjusts automatically so that the CFL condition is always satisfied regardless of the configuration of the grid.

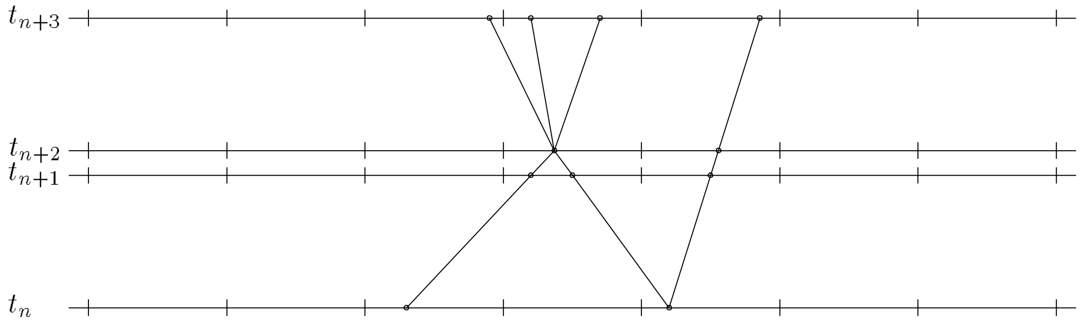


FIG. 1. *A typical grid in the $x$-$t$ plane when shock-tracking is used to model the collision of two shocks with the Euler equations. The uniform grid is augmented by cell interfaces at the discontinuities. The time step is adjusted so that the shock collision is correctly resolved.*

Figure 1 shows a typical grid over several time steps. In this case there are two tracked discontinuities which interact at some point. One important feature of our method is that we adjust the time step when required so that collision of tracked discontinuities occurs exactly at the end of a time step. As a result, the solution of the Riemann problem in the next time step gives the exact resolution of the collision into outgoing waves. For example, Figure 1 shows the collision of two gas dynamic shocks modeled with the Euler equations, resulting in two outgoing shocks and a contact discontinuity. All three waves are then tracked after the collision.

More details of this algorithm and additional numerical results can be found in the technical report [27]. A sequel paper on two-dimensional front tracking is in preparation. More details on both the one-dimensional and the two-dimensional algorithm can be found in the second author's thesis[36].

**2. Approaches to shock tracking.** A wide variety of approaches have been used over the years to develop shock tracking or interface tracking methods. We will only mention a few of the main ideas used in one space dimension and how they relate to our method. A concise survey of several approaches for the multi-dimensional problem is given by Hyman[16]. See also Finlayson[12] and Oran and Boris[32] for discussions of specific applications.

One approach is to solve the differential equations separately on each side of the discontinuity using a method designed for smooth flow, while the shock or interface is handled in a different manner using the Rankine-Hugoniot jump conditions. For example, Mao[29] has recently introduced a method of this type in which two sets of data near the interface are constructed by extrapolating the data from each side to the other side. High resolution ENO (essentially non-oscillatory) methods are applied to the extrapolated values which now define smooth functions. The method is not exactly conservative at the interface, although errors in conservation appear to be small. This has also been extended to two space dimensions in an interesting way using dimensional splitting[30].

Another approach in one dimension is to represent the flow entirely by a collection of discontinuities, all of which are explicitly tracked. Following Dafermos[9], a piecewise linear equation of state is used to ensure that only discontinuities arise in solutions to Riemann problems. This approach has been used by Hedstrom[15] and by Swartz and

Wendroff[39] and has more recently been adopted by Risebro and Tveito[33],[34]. Since every collision must be explicitly handled by solving a Riemann problem, and the collision of two waves typically gives rise to $m$ new waves (for a system of $m$ equations), this can clearly lead to an explosion of information if $m > 2$, as in the Euler equations. (Although Wendroff[43] has studied this method for a problem arising in chromatography and shows that for this special system the number of waves remains bounded.) In general, at some point weak waves must be suppressed in order to limit the amount of information retained, leading to a loss of conservation. Another problem is that smooth flow is not represented with high order accuracy. Finally, there is the obvious difficulty of extending such methods to more than one dimension.

Our method is perhaps closest to that of Chern and Colella[5]. They also use a conservative method on a uniform grid, with some grid cells subdivided by the tracked front. They avoid stability problems in small partial cells by a "flux redistribution" algorithm that modifies fluxes at the boundaries of these and neighboring cells in such a way that stability is restored while conservation is maintained. Our use of the wave propagation algorithm described in the next section has the same effect. In addition, we believe it to be more solidly based on the correct physical behavior of the waves, and more amenable to higher order extensions and theoretical analysis.

Another way to deal problematical small cells is to eliminate them by merging them with adjacent cells, temporarily eliminating a "fixed" cell boundary in the process. This approach is used, for example, in [31] and [39]. However, this may be impossible to do if several tracked fronts fall within one fixed grid cell. Moreover, this seems to be unnecessary with our approach.

Finally, we want to mention that there are also a number of shock capturing approaches that are capable of improving the resolution of discontinuities. Methods of this type include the self-adjusting grid methods of Harten and Hyman[14], and the ENO method with subcell resolution of Harten[13].

**3. High resolution wave propagation methods.** We begin by discussing the high resolution numerical method that is used to compute the smooth flow. Although this method is related to various flux-limiter or MUSCL methods that have been widely used for conservation laws, the formulation is somewhat different. We use a wave-propagation viewpoint that extends easily to the case of shock tracking and maintains stability even when very small cells are created.

We describe the method on a general irregular grid with grid spacing $h_j = x_{j+1} - x_j$. We use a finite-volume formulation in which the value $U_j^n$ approximates the cell average of the solution over the grid cell $[x_j, x_{j+1}]$ at time $t_n$,

$$U_j^n \approx \frac{1}{h_j} \int_{x_j}^{x_{j+1}} u(x, t_n)\, dx.$$

The time step is denoted by $k$. Note that the grid may vary from step to step but the method involves only two time levels, so this presents no difficulty.

The methods we use are based on solving Riemann problems at each interface $x_j$ with data $U_{j-1}^n$ and $U_j^n$. (See [24] for an overview of such methods.) Rather than computing the exact solution to the Riemann problem, which can be done for practical problems such as the Euler equations but is rather expensive, we use an approximate solver developed by

Roe[35] at most interfaces. This is much more efficient to compute than the exact Riemann solution and in smooth regions of the flow provides a very accurate approximation. Only at shock collision points do we use the exact Riemann solver so that the nonlinear interaction is accurately computed (see Section 4 for further discussion).

Roe's approximate Riemann solver replaces the nonlinear equation $u_t + f(u)_x = 0$ with data $u_l$ and $u_r$ by a linear system

$$u_t + \hat{A}(u_l, u_r)u_x = 0. \tag{3.2}$$

The matrix $\hat{A}(u_l, u_r)$ is chosen to have the following properties:

$$\begin{aligned} &i) \quad \hat{A}(u_l, u_r)(u_r - u_l) = f(u_r) - f(u_l) \\ &ii) \quad \hat{A}(u_l, u_r) \text{ is diagonalizable with real eigenvalues} \\ &iii) \quad \hat{A}(u_l, u_r) \to f'(\bar{u}) \text{ smoothly as } u_l, u_r \to \bar{u}. \end{aligned} \tag{3.3}$$

Such matrices have been derived for several systems of practical interest. For the Euler equations with a $\gamma$-law gas, the form of the matrix is given by Roe[35].

The solution of the linear system (3.2) is a similarity solution that consists of $m$ discontinuities propagating at constant speeds. The jump across each discontinuity is an eigenvector of the matrix $\hat{A}$, and the propagation speed is the corresponding eigenvalue. We thus have

$$u_r - u_l = \sum_{p=1}^{m} r_p, \tag{3.4}$$

where $r_p \in \mathbb{R}^m$ is an eigenvector of $\hat{A}$,

$$\hat{A} r_p = \lambda_p r_p, \quad p = 1, 2, \ldots, m.$$

Wave propagation methods are based on using these propagating discontinuities to update the cell averages in the cells neighboring each interface. Condition (3.3 $i$) guarantees that the method remains conservative.

To begin, we assume that these waves affect only the cells adjacent to the discontinuity during the time step. This requires that the Courant number be less than 1. The Courant number $\nu$ is defined by

$$\nu = \frac{k}{h_{\min}} \max_{p,j} |\lambda_{pj}| \qquad \text{where} \qquad h_{\min} = \min_j h_j \tag{3.5}$$

and $\lambda_{pj}$ represents the $p$th eigenvalue obtained from the Riemann problem at $x_j$. Note that $k\lambda_{pj}$ is the distance a wave propagates during the time step. If $\lambda_{pj} < 0$ then we need $k|\lambda_{pj}| < h_{j-1}$ while if $\lambda_{pj} > 0$ we need $k\lambda_{pj} < h_j$ in order that the wave stays within the adjacent cell. Condition (3.5) is sufficient to guarantee this.

**Godunov's method.** A first order accurate version of the wave propagation method is then equivalent to Godunov's method, with the Roe Riemann solver, on an irregular grid. That is to say, we solve the Riemann problems at each interface over a time step of length $k$ and then average the resulting solution over the grid cells to obtain $U^{n+1}$. By computing the effect of each wave on the cell average, we obtain the wave-propagation

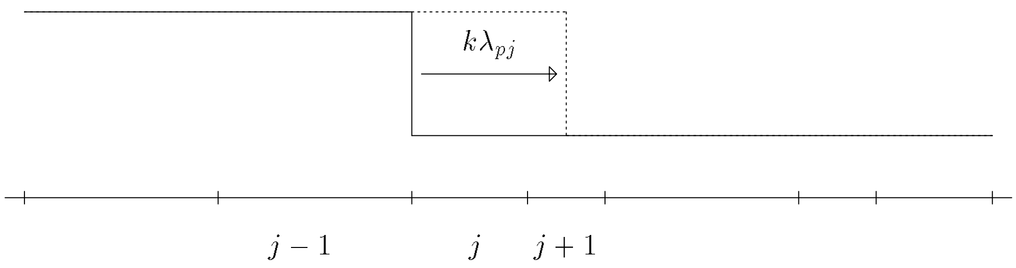


FIG. 2. *Wave propagation in the case $k\lambda_{pj} > h_j$. The wave propagates entirely through one cell and part way through the neighbor.*

form of the method. We first initialize $U_j^{n+1} := U_j^n$ in all cells and then at each interface $x_j$ we apply the following updates:

$$\begin{aligned} &\text{For } p = 1,\ 2,\ \ldots,\ m \text{ do} \\ &\quad \text{If } \lambda_{pj} < 0 \text{ then } i := j-1 \text{ else } i := j \\ &\quad U_i^{n+1} := U_i^{n+1} - \left(\frac{k\lambda_{pj}}{h_i}\right) r_{pj} \end{aligned}$$

We can rewrite this method as a standard finite difference method in conservation form if we look at the total contribution to each grid cell. This is described in detail in [18], [21]. The advantage of using the wave propagation form rather than the more traditional flux differencing form is that the method can then be easily extended to the case where the Courant number is larger than 1.

For example, if $k|\lambda_{pj}| > h_j$ at some point in the algorithm, then the corresponding wave should update more than one cell average, as shown in Figure 2. In this figure, $U_j^{n+1}$ is updated by the entire jump $r_{pj}$,

$$U_j^{n+1} := U_j^{n+1} - r_{pj},$$

while $U_{j+1}^{n+1}$ is updated by

$$U_{j+1}^{n+1} := U_{j+1}^{n+1} - \left(\frac{k\lambda_{pj} - h_j}{h_{j+1}}\right) r_{pj}.$$

The method remains conservative with this modification[18]. This "large time step" version of Godunov's method is discussed in some detail in [19].

Note that each wave is propagated independently of all other waves. When the Courant number is larger than 1, waves should perhaps interact with one another and only for linear systems of equations is it really correct to propagate them independently. For nonlinear problems there should be a change in the strength and speed of each wave after any collision. In spite of this, the "linearization" that we use works quite well in the context of shock tracking. As explained in the next section, the interaction of two strong discontinuities is handled exactly by modifying the time step, and so at least one of the waves involved is a weak wave coming from the smooth flow. For the interaction of weak waves, this linearization has been analyzed in [22].

Regarding stability, we note that for a scalar nonlinear conservation law the method is total variation diminishing (TVD) and hence is stable and convergent[18]. Also, for a linear system of conservation laws the method reduces to a scalar large time step method on each field and again is stable. For nonlinear systems of equations, some oscillation problems have been observed when large Courant numbers on uniform grids are used in the context of shock capturing[19]. In this case the Courant number is large everywhere and the linearization of the nonlinear interactions between strong waves apparently gives difficulties. However, in the context of shock tracking, where the Courant number is large only due to occasional small cells and we are capturing smooth flow, we have not observed stability problems for most calculations. In one example presented in Section 7, the Woodward-Colella blast wave interaction problem, we have experienced difficulties due to negative pressures using the linear wave interactions. This is an extreme case in which a strong rarefaction wave overtakes a shock that has a very low pressure in front of it. The pressure becomes negative when the rarefaction wave passes through the blast wave and enters the low pressure region. In Section 7, we outline one possible way to handle this difficulty, at the expense of some complication of the algorithm.

**High resolution modifications.** We now extend the method to a high resolution method, *i.e.*, a method that achieves second order accuracy on smooth flows (except perhaps near extrema) and also avoids oscillations near discontinuities. The approach we use is similar to the MUSCL approach of van Leer[42] in that we introduce piecewise linear approximations to the solution in place of the piecewise constant functions used in Godunov's method, but the form of the method is quite different and allows easy extension to the case where the Courant number is larger than 1.

We begin by solving the Riemann problems as before, using the piecewise constant data. The resulting jumps $r_{pj}$ are then used to obtain slope information in each characteristic family. Let

$$h_{j-1/2} = \frac{1}{2}(h_{j-1} + h_j)$$

be the distances between cell centers. Note that

$$\begin{aligned} \sum_{p=1}^{m} r_{pj}/h_{j-1/2} &= (U_j^n - U_{j-1}^n)/h_{j-1/2} \\ &= u_x(x_j, t_n) + O(h). \end{aligned}$$

So each component $r_{pj}/h_{j-1/2}$ is the contribution to the slope arising from the $p$th family. It is important to decompose the slope into components, since the waves in the different families propagate at different speeds and perhaps in different directions. Moreover, when we introduce slope limiting we will do the limiting separately in each family. We wish to limit slopes near a discontinuity in order to avoid oscillations, but wish to do this in the family with the discontinuity without affecting accuracy in other families where the solution may be smooth.

We will use $\sigma_{pj}$ to denote the slope used in the $p$th family over the cell $[x_j, x_{j+1}]$. The unlimited slope is taken to be

$$\sigma_{pj} = \begin{cases} r_{pj}/h_{j-1/2} & \text{if } \lambda_{pj} < 0 \\ r_{p,j+1}/h_{j+1/2} & \text{if } \lambda_{p,j+1} > 0. \end{cases} \tag{3.6}$$

To avoid oscillations, the slope $\sigma_{pj}$ should be chosen based on a slope limiter. If we let $\sigma_{pj}^{(i)}$ be the $i$th component of $\sigma_{pj}$ $(i = 1, 2, \ldots, m)$ and similarly let $r_{pj}^{(i)}$ be the $i$th component of $r_{pj}$, then we apply a slope limiter separately in each component, *i.e.*, we take

$$\sigma_{pj}^{(i)} = \phi(\theta_{pj}^{(i)}) \left( \frac{r_{pj}^{(i)}}{h_{j-1/2}} \right) \tag{3.7}$$

where $\phi$ is some limiter function applied to the slope ratio

$$\theta_{pj}^{(i)} = \frac{r_{p,j+s}^{(i)}/h_{j+s-1/2}}{r_{pj}^{(i)}/h_{j-1/2}}, \tag{3.8}$$

with $s = -\text{sgn}(\lambda_{pj})$. Any standard limiter can be used, *e.g.*, the well-known "minmod" or "superbee" functions. See Sweby[40] for a general discussion of limiters.

This slope is used to modify the cell averages computed *via* the first order algorithm. The modification is accomplished by shifting a certain mass between cells in a conservative manner. The idea is best explained by considering the linear advection equation

$$u_t + au_x = 0 \tag{3.9}$$

on a grid with Courant number $\nu = ak/h_{\min} \leq 1$, $a > 0$. Godunov's method is then simply the first order upwind method

$$U_j^{n+1} = U_j^n - \frac{ak}{h_j}(U_j^n - U_{j-1}^n). \tag{3.10}$$

This can be interpreted as follows: view $U_j^n$ as defining a piecewise constant function $\tilde{u}(x, t_n)$. Shift this function at the propagation speed $a$ to obtain $\tilde{u}(x - ak, t_n)$. Now average this function over the grid cells to obtain

$$U_j^{n+1} = \frac{1}{h_j} \int_{x_j}^{x_{j+1}} \tilde{u}(x - ak, t_n)\, dx.$$

It is easy to verify that this gives (3.10). The cell average is updated by the shaded area in Figure 3a divided by the cell length.

A natural way to extend this to second order accuracy is to replace the piecewise constant function by a piecewise linear function with slopes $\sigma_j$ on each cell as obtained, for example, from (3.6). For the scalar equation this reduces to

$$\sigma_{j-1} = (U_j^n - U_{j-1}^n)/h_{j-1/2}. \tag{3.11}$$

We then shift this function at speed $a$ and average onto the grid. We thus obtain $U_j^{n+1}$ by updating $U_j^n$ according to the shaded area of Figure 3b. An easy way to accomplish this is to split the procedure into two pieces. In the first step we update cell averages using the piecewise constant wave as in Figure 3a (*i.e.*, we apply (3.10)), and in the second step we propagate the piecewise linear wave form shown in Figure 3c, with zero mean value and slope $\sigma_{j-1}$ over the $(j-1)$ cell. We then further update $U_j^{n+1}$ by the shaded area in Figure 3c, *i.e.*, we set

$$U_j^{n+1} := U_j^{n+1} + \frac{ak}{2h_j}(h_{j-1} - ak)\sigma_{j-1}.$$

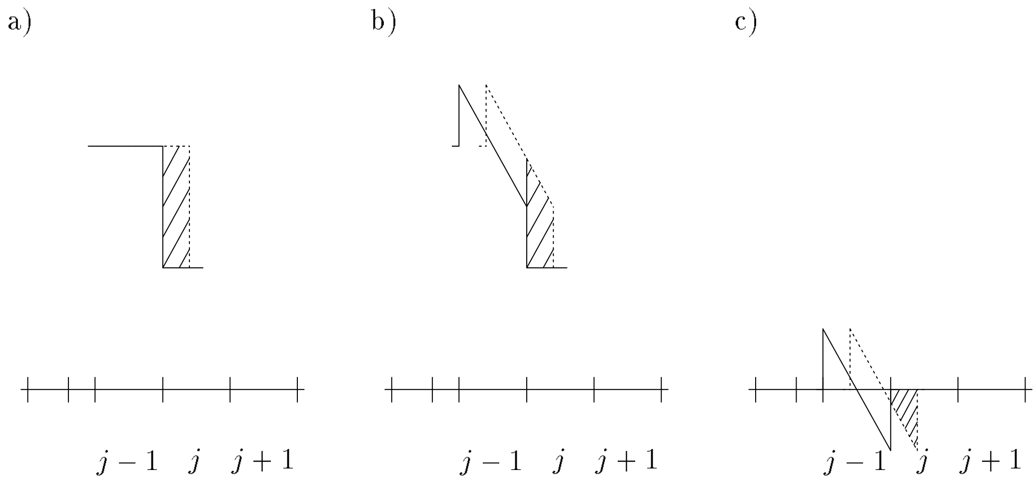


FIG. 3. *a) Propagation of the piecewise constant wave. b) Propagation of a piecewise linear wave form. c) Second order correction wave. The propagation shown in Figure b) can be decomposed into propagation of the piecewise constant wave of Figure a) together with propagation of this correction wave.*

We also update $U_{j-1}^{n+1}$ by the area of the portion of the correction wave that overlaps this cell,

$$U_{j-1}^{n+1} := U_{j-1}^{n+1} - \frac{ak}{2h_{j-1}}(h_{j-1} - ak)\sigma_{j-1}.$$

Conservation is maintained in this correction step with any choice of slopes since the above two corrections (weighted by cell size) sum to zero.

Of course $U_j^{n+1}$ will also be updated by the wave originating from $x_{j+1}$. When all of these updates are combined, we find that

$$U_j^{n+1} = U_j^n - \frac{ak}{h_j}(U_j^n - U_{j-1}^n) + \frac{ak}{2h_j}(h_{j-1} - ak)\sigma_{j-1} - \frac{ak}{2h_j}(h_j - ak)\sigma_j.$$

On a regular grid with slopes (3.11), this reduces to the Lax-Wendroff method for the advection equation and is second order accurate.

The extension to nonlinear systems is straightforward. We apply this same technique in each wave family, indexed by $p$. In the case where $|k\lambda_{pj}/h_i| \le 1$ for $i = j-1$ and $j$ this slope affects only these two cells and the updates are given by

$$\text{If } \lambda_{pj} < 0 \text{ then } i := j \text{ else } i := j-1$$

$$U_j^{n+1} := U_j^{n+1} + \frac{k|\lambda_{pj}|}{2h_j}(h_i - |\lambda_{pj}|k)\sigma_{pi}$$

$$U_{j-1}^{n+1} := U_{j-1}^{n+1} - \frac{k|\lambda_{pj}|}{2h_{j-1}}(h_i - |\lambda_{pj}|k)\sigma_{pi}$$

The advantage of the wave propagation form of this second order correction is that generalization to nonuniform grids and Courant numbers larger than 1 is again straightforward. We simply average the correction wave shown in Figure 3c onto whatever grid cells it overlaps. In general there may be more than two such cells. Further description of this approach can be found in [21] and [23].

For a scalar nonlinear problem on a regular grid with slopes (3.6), this again reduces to a form of the Lax-Wendroff method and can easily be verified to be second order accurate. For a nonlinear system of equations on a uniform grid, this method is quite comparable to other slope limiter or flux limiter methods and yields similar high quality results[21].

**4. The shock tracking algorithm.** Our grid consists of two parts. We choose a uniform, underlying grid with mesh size $h$ that remains fixed for all time, and we also introduce tracked points which vary from step to step. These tracked points subdivide some regular cells into two or more subcells, creating some irregular cells. We then view the union of the regular cells and irregular cells as our global grid (recall Figure 1). In each grid cell the cell average is denoted by $U_j^n$.

In each time step our shock tracking algorithm consists of the following steps:

**1)** Determine the size of the next time step and the location of the tracked points at the next time step.
**2)** Modify the current grid by inserting these new tracked points. Some cells will be subdivided and the values in each subcell must be initialized.
**3)** Take a time step on this irregular grid using the algorithm described in Section 3 to update the cell averages.
**4)** Delete the old tracked points from the previous time step. Some subcells will be combined and a value in the combined cell must be determined from the subcell values.

Before describing each of these steps in more detail, we first discuss some possible approaches to setting up the data structure. One possibility is to use a doubly linked list for the entire grid (see [1] or [17] for more information on the use of linked lists). Each grid cell is an element of this list, with pointers to the previous and next grid cells. With this data structure it is easy to insert and delete grid points and the distinction between regular and irregular cells disappears. This is reasonable in Step 3 of our procedure, where little distinction is made between regular and irregular cells, although we will see that we must be careful in our choice of slopes near tracked points. We also need to keep track of which points must be deleted in Step 4. For these reasons we would also maintain a flag for each point that tells whether it is a regular point, an old tracked point, or a new tracked point.

The use of doubly linked list does not extend very well to two space dimensions. Another more general approach is to use a standard representation for the fixed grid together with a flag for each grid cell that indicates whether the grid cell is subdivided by one or more tracked points. For subdivided cells, this flag can be a pointer to another data structure containing information on each subcell. This latter data structure also interfaces more easily with the adaptive mesh refinement algorithm we use, and so we have taken this approach in our code.

We now discuss each step of this algorithm in more detail.

**Step 1:** We begin our algorithm by solving the Riemann problem at each interface and obtain the resulting jumps $r_{pj}$ and speeds $\lambda_{pj}$. Then at each interface we check each jump $r_{pj}$ to see if it should be tracked. This can be done by checking, for example, if the max-norm of $r_{pj}$ is greater than some prescribed tolerance $\varepsilon$, or if the jump in some physically meaningful variable (*e.g.*, density or entropy) is greater than the tolerance $\varepsilon$. The choice of the checking criterion and tolerance $\varepsilon$ for determining the tracked waves may depend on the specific problem and should be adjusted accordingly. In order to capture shock formation, the jumps have to be checked at regular interfaces as well as at the tracked interfaces so that new tracked points can be introduced. By examining the jumps at the tracked interfaces, decaying shocks can also be detected and hence ignored.

Only waves corresponding to the physically relevant discontinuities should be tracked, *i.e.*, shocks or contact discontinuities. Although rarefaction waves are also approximated by discontinuities in the Roe Riemann solver, we want them to be smeared rather than remaining sharp and so they should not be tracked even if their strength is greater than $\varepsilon$. Moreover, due to this rarefaction wave approximation, we may obtain an entropy-violating solution if the rarefaction wave is a transonic one. This entropy violation can be fixed in various ways, for example by replacing the single entropy-violating discontinuity by two discontinuities traveling in opposite directions[14].

Before entering the shock tracking algorithm, we have some basic time step $k$. In order to avoid the interaction of tracked waves during this time step, we adjust our time step if needed. It will be adjusted in such a way that the collision of two tracked waves occurs exactly at the end of a time step (recall Figure 1). This can be accomplished quite easily, by checking the collision times of all adjacent tracked waves.

If collision occurs, in the next time step the approximate Riemann solver is replaced by the exact Riemann solver at the collision point to insure that the resulting waves in the next time step are well resolved. By choosing the time step in this way and using the exact Riemann solver, we guarantee that the collision of two tracked waves is always handled correctly.

**Step 2:** After choosing the time step $k$ we can compute the locations of each tracked wave at the end of the time step. Some of these locations may coincide if two waves collide, or if the new locations are exactly at the old grid interfaces. Also, some waves may pass outside of our computational domain at an outflow boundary. For each distinct wave location in the domain, we insert a new cell interface into our old grid. Each new point subdivides some cell into two subcells. We must assign a cell value to each of these subcells. (see Figure 4 for an example). The simplest approach is to assign the previous cell value to each subcell. It would be preferable to use some form of interpolation to determine more accurate values on these cells. However, doing so would change the solutions to neighboring Riemann problems and perhaps the speed of the tracked waves. The location of the point we are inserting might therefore be incorrect. For this reason we use the simpler approach.

**Step 3:** Once the new grid is constructed, the cell average values $U_j^n$ are then updated by applying the numerical method described in Section 3 (see Figure 5 for illustration). Since the new grid has been chosen carefully so that all the strong waves are propagated exactly to cell boundaries, there is no smearing of the tracked waves during the averaging process. Smooth flow is captured as usual. Note that during this propagation process, all waves are propagated independently, and in principle no distinction need be made between tracked points and ordinary grid boundaries. Near tracked points, waves may propagate through several cells due to the fact that we have created small subcells. A consequence of this is that waves pass through one another as they would in a linear equation, without undergoing the nonlinear interaction that should occur. For weak waves, this is a good

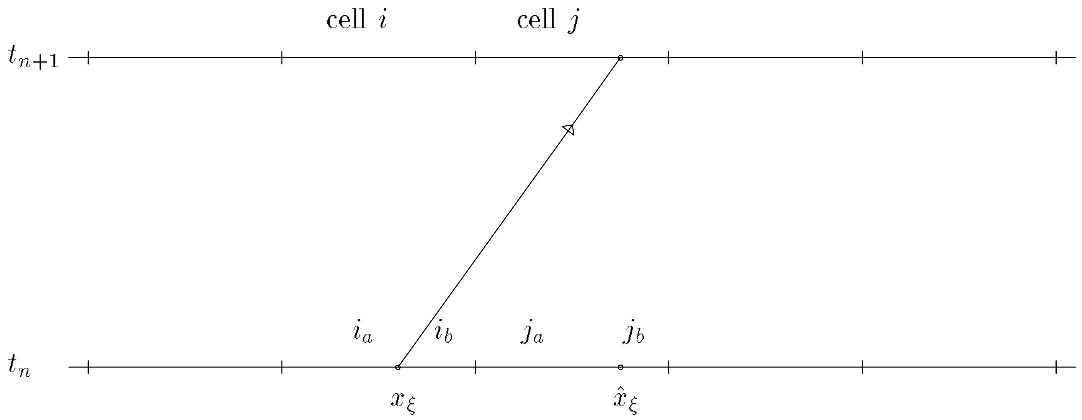


FIG. 4. *A shock propagating from cell $i$ to cell $j = i+1$ leads to a subdivision of cells $i$ and $j$. In time step $n$ we split cell $j$ in two, setting $U^n_{j_a} = U^n_{j_b} = U^n_j$. In time step $n+1$ we eliminate the old tracked point in cell $i$, using (4.12).*

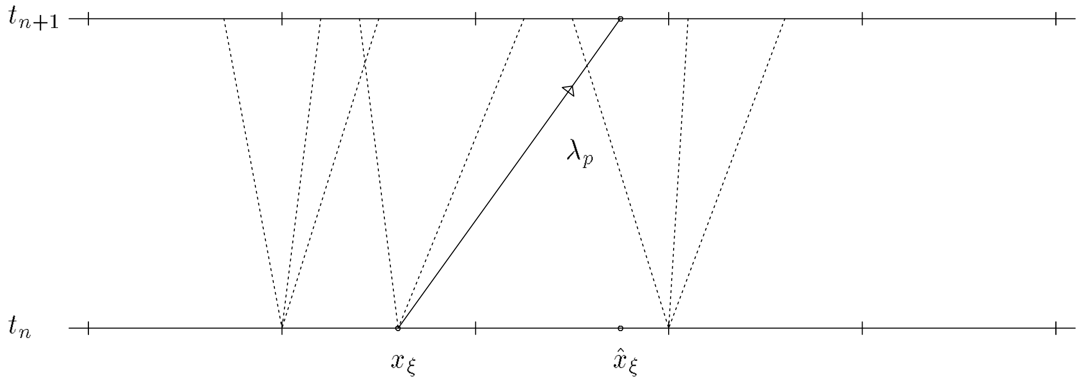


FIG. 5. *Wave propagation in Step 3. Each wave is propagated independently, and for waves passing through each other the interaction is linearized. Note that the tracked wave is propagated exactly to the new cell boundary $\hat{x}_\xi$ introduced in Step 2. (The solid line represents the tracked wave, and the dashed lines are the weak waves.)*

approximation, as described in [19]. For the interaction between a strong tracked wave and the weak waves arising from nearby Riemann problems, this linearization is less valid. In general this does not seem to give any difficulties, although for the blast wave interaction problem considered in Section 7 we must compute some of these interactions correctly in order to avoid nonphysical negative pressures arising. This is discussed further in Section 7.

**Step 4:** We now delete the old tracked points from the current grid. This corresponds to merging two subcells into one, and the cell value in the combined cell is calculated by the appropriate weighted combination of these two deleted subcells to maintain the correct cell average. For example, in Figure 4 the old tracked point $x_\xi$ is deleted from the $i$th regular cell and the $i$th cell average after deletion becomes

$$U_i^{n+1} := \frac{x_\xi - x_i}{h} U_{i_a}^{n+1} + \frac{x_{i+1} - x_\xi}{h} U_{i_b}^{n+1} \tag{4.12}$$

where $U_{i_a}^{n+1}$, $U_{i_b}^{n+1}$ are the cell averages in the first and second subcell of the $i$th cell respectively, and $h$ is the underlying fixed mesh size.

**Improved slopes.** The high resolution method described in Section 3 can be used directly on the nonuniform grid generated by the uniform grid together with the appropriate tracked points. It turns out that we can do better, however, by taking advantage of the fact that we know that large jumps in the solution should appear at the tracked points whereas the nearby flow should be smooth. High resolution methods using limiters were originally developed for shock capturing methods where a shock will typically be smeared over several grid points. Since reasonable slope information may be unavailable in this region, limiting the slope to a value near zero may be appropriate. In the present context, however, we might expect to have meaningful slope information in the cells near the discontinuity.

Consider a cell $j$, for example, where the interface to the right is a tracked point and interfaces to the left are regular grid interfaces. The solution to the Riemann problem on the right, at the tracked point, should clearly not be used to estimate a slope over this grid cell for the family of the tracked wave. Waves arising from the Riemann problem to the left may give a very useful slope estimate, however. Since it is still valuable to compare adjacent slopes *via* a limiter in case other discontinuities are present that are not being tracked, we choose $\sigma_j$ based on a one-sided formula similar to (3.7) but using the waves $r_{pj}$ at the boundary to the left and the waves $r_{p,j-1}$ at the left boundary of the adjacent cell.

This choice of slopes is particularly important if we wish to solve problems where the solution has an extremum at the discontinuity. This occurs in many applications, *e.g.*, in the combustion problem presented later. If we are not careful about the choice of slopes near the discontinuity, these extreme points will be severely clipped. This effect and the benefit obtained by introducing one-sided slopes near tracked points is investigated in Section 9.

**5. The Euler equations and boundary conditions.** Before presenting numerical results obtained with this shock tracking algorithm, we pause to introduce the Euler equations of gas dynamics and discuss the implementation of boundary conditions for this system.

The inviscid Euler equations of gas dynamics in one space dimension take the form

$$\frac{\partial}{\partial t}\begin{pmatrix}\rho\\ \rho v\\ \rho E\end{pmatrix}+\frac{\partial}{\partial x}\begin{pmatrix}\rho v\\ \rho v^2+p\\ (\rho E+p)v\end{pmatrix}=0, \tag{5.13}$$

where $\rho, v, p, E$ are the density, velocity, pressure, and total energy of the gas per unit mass, respectively. We assume that the equation of state satisfies the $\gamma$-law, where $\gamma$ is the ratio of specific heats ($\gamma \cong 1.4$ for air). Then the internal energy is $e = \frac{1}{\gamma-1}p/\rho$ and $E = e + \frac{1}{2}v^2$. The three components of Equations (5.13) express the conservation of mass, momentum, and energy, respectively[8].

Outflow boundary conditions are easily achieved with the wave propagation approach by simply ignoring waves once they leave the computational domain, and by not introducing any new waves at the boundary.

At a solid wall boundary, say at $x = 0$, we have the no-flow boundary condition

$$v(0,t) = 0.$$

This boundary can be treated as a line of symmetry. If we reflect our grid near the boundary to the region $x < 0$, we can assign grid values in the reflected cells using

$$U_{-j}^n = \mathcal{R}(U_j^n), \quad j = 1,\ 2,\ \ldots$$

where $\mathcal{R}$ represents the operator that negates the second component of $U$ (the momentum) while leaving the first and third (density and energy) unchanged. Applying the algorithm over a slightly extended domain simulates the solid wall boundary condition.

Alternatively, we can avoid extending the grid if we note that each incoming wave (a wave entering our true computational domain from $x < 0$) can be viewed as the reflection of an outgoing wave (a wave crossing $x = 0$ with negative speed). This is illustrated in [21], [23]. The relation between the reflected jump $\bar{r}_{pj}$ and the outgoing jump $r_{pj}$ is simply

$$\bar{r}_{pj} := -\mathcal{R}(r_{pj})$$

and the speed of the reflected wave is $\bar{\lambda}_{pj} = -\lambda_{pj}$. Hence we need only solve Riemann problems on our original grid and then reflect any waves that hit the boundary. In the high resolution version, we must also reflect the outgoing slope in the same way,

$$\bar{\sigma}_{pj} := -\mathcal{R}(\sigma_{pj}).$$

In addition, we must solve a boundary Riemann problem with data $u_r = U_1^n$ given by the cell adjacent to the boundary and $u_l = \mathcal{R}(u_r)$. There is one incoming wave that affects the grid values (the contact discontinuity will have speed zero by symmetry and the outgoing wave is ignored).

This wave reflection procedure is quite easy to implement, and is applicable for any mesh size and any time step.

Finally, we discuss how this reflection procedure can be applied to a moving boundary, e.g., a moving piston. We approximate the piston motion by assuming that the velocity is constant within each time step. Assume that the piston is located at $x = z_n$ at time

$t_n$ and is moving with speed $s_n$ for $t_n \le t \le t_{n+1}$. Then the physically correct boundary condition is

$$v(z_n + s_n(t - t_n), t) = s_n$$

for $t_n \le t \le t_{n+1}$. Using the Galilean transformation, we can derive that

$$\begin{aligned} \rho(z_n-) &= \rho(z_n+) \\ v(z_n-) &= 2s_n - v(z_n+) \\ p(z_n-) &= p(z_n+) \end{aligned} \tag{5.14}$$

is the correct data for the boundary Riemann problem. This defines a generalization of the reflection operator $\mathcal{R}$. Determining the corresponding reflection of the energy, we find that a jump which hits the boundary should now be reflected using the following relations:

$$\begin{aligned} \bar{r}_{pj}^{(1)} &= -r_{pj}^{(1)} \\ \bar{r}_{pj}^{(2)} &= r_{pj}^{(2)} - 2s_n r_{pj}^{(1)} \\ \bar{r}_{pj}^{(3)} &= -r_{pj}^{(3)} + 2s_n r_{pj}^{(2)} - 2(s_n)^2 r_{pj}^{(1)}. \end{aligned} \tag{5.15}$$

For shorthand, we write $\bar{r}_{pj} = -\mathcal{R}_n(r_{pj})$. The reflected slopes can be determined by the same reflection, $\bar{\sigma}_{pj} = -\mathcal{R}_n(\sigma_{pj})$. The reflected speed $\bar{\lambda}_{pj}$ is simply equal to $2s_n - \lambda_{pj}$.

**6. A double piston problem.** Consider a shock tube with unit length and two pistons moving from the left and right boundaries into the stationary gas ($\gamma = 1.4$) with $\rho = 1.4$ and $p = 1$. We choose smooth piston velocities $s_p(t)$ of the form

$$s_p(t) = \begin{cases} \kappa_1 t & t \le t_1 \\ \frac{\kappa_2(t_2 - t)}{\sqrt{r^2 - (t_2 - t)^2}} & t_1 < t \le t_2 \\ 0 & t > t_2. \end{cases}$$

The parameters for each piston are given by:

left piston: $\kappa_1 = 5,\ \kappa_2 = 1,\ t_1 = 0.31,\ t_2 = 0.444$

right piston: $\kappa_1 = -4,\ \kappa_2 = -1,\ t_1 = 0.42,\ t_2 = 0.557$

and $r = 0.16$ in each case.

Two compression waves arise from the left and right pistons and eventually form shock waves, which subsequently interact. Two outgoing shocks result from the interaction, and begin to interact with the rarefaction waves and the pistons. The rarefaction waves result from stopping the pistons (see Figure 6b).

In the numerical method, we replace the piston path by a piecewise constant path, using the constant velocity $s_p(t_n + \frac{1}{2}k)$ over the time interval $t_n \le t \le t_{n+1}$, where $k$ is the time step. Then the piston boundary conditions described in Section 5 are applied to each piston. In Figure 6a, we show the tracked points, which include the location of the tracked shocks and the pistons' paths, by using the high resolution shock tracking algorithm with $h = 1/100$, Courant number $\nu = 0.9$ (relative to the uniform cells), and the "minmod" slope limiter. We track waves for which the density jump is greater than the tolerance $\varepsilon = 1$. It is clearly seen that the shock formation and tracked wave interactions are handled quite well by our shock tracking algorithm.

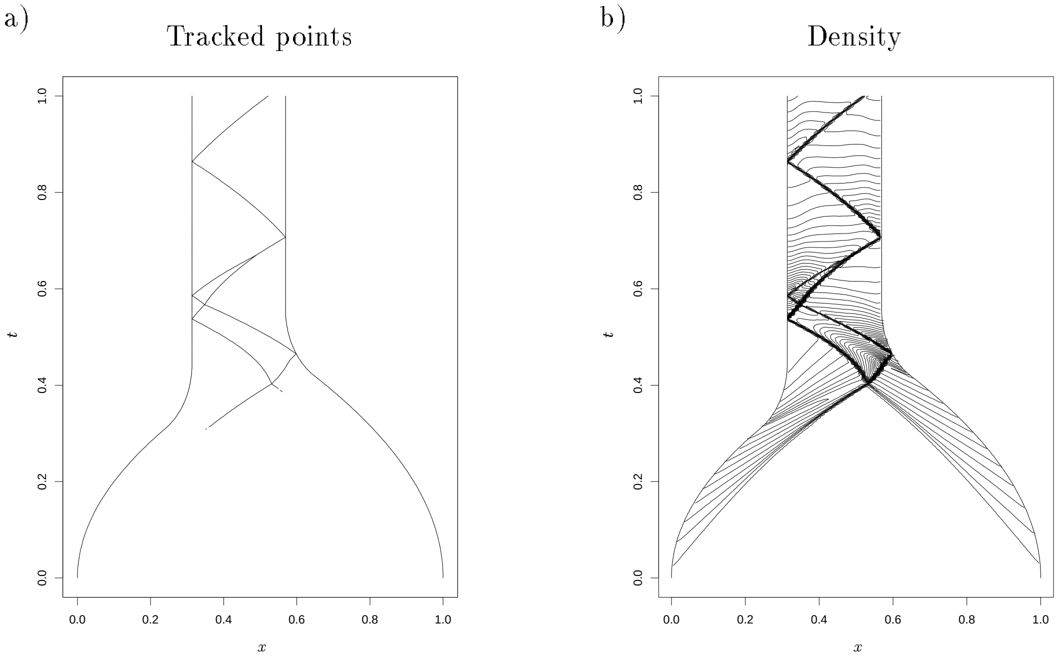


FIG. 6. *a) Tracked points for the double piston problem. b) The density contour plot in the $x$-$t$ plane.*

The density contour plot in the $x$-$t$ plane is shown in Figure 6b for the same run. From it, we can see that numerous wave interactions occur. The linear wave interaction is used for the interaction of tracked shocks with the background smooth flow and gives satisfactory results. In Figure 7 we compare our numerical result ($h = 1/100$) with a fine grid solution ($h = 1/800$ and shock tracking) at time $t = 0.6$, observing good agreement.

From this test problem, we see that our shock tracking algorithm is capable of handling shock formation, moving boundaries, and wave interactions.

**7. The Woodward-Colella problem.** As our next example we consider the blast wave interaction problem studied by Woodward and Colella[45],[46]. In this problem the initial condition consists of three constant states with data

$$\begin{pmatrix} \rho \\ v \\ p \end{pmatrix}_l = \begin{pmatrix} 1 \\ 0 \\ 10^3 \end{pmatrix}, \quad \begin{pmatrix} \rho \\ v \\ p \end{pmatrix}_m = \begin{pmatrix} 1 \\ 0 \\ 10^{-2} \end{pmatrix}, \quad \begin{pmatrix} \rho \\ v \\ p \end{pmatrix}_r = \begin{pmatrix} 1 \\ 0 \\ 10^2 \end{pmatrix},$$

where $l$ is the state used for $x \in [0, 0.1)$, $m$ is the state used for $x \in [0.1, 0.9)$, and $r$ is the state used for $x \in [0.9, 1]$. The gas we consider satisfies the $\gamma$-law gas with $\gamma = 1.4$. There are two solid walls at $x = 0$ and $x = 1$.

With this initial condition a shock wave, contact discontinuity, and rarefaction wave develop at each discontinuity individually. The shock waves are moving toward each other and then collide. A new contact discontinuity arises from the collision. Further collisions then occur. A density contour plot in the $x$-$t$ plane is shown in Figure 8 which indicates the complex wave pattern of this problem.

The most difficult part of this problem is the very low pressure in the middle state. Any small perturbation caused by numerical error can lead to negative pressures. There-

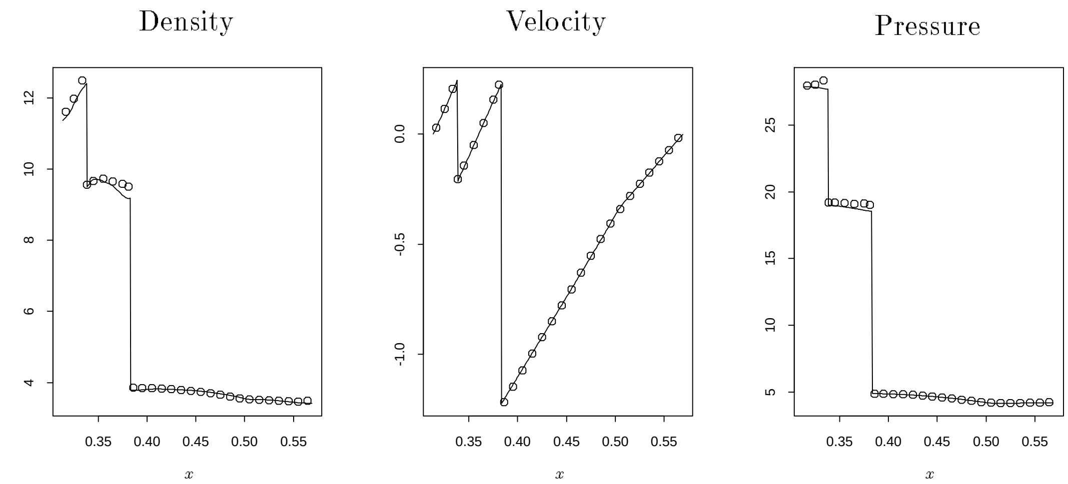


FIG. 7. *Comparison plots for the double piston problem at time $t = 0.6$. In each figure the solid line is the fine grid solution with $h = 1/800$ and the points show the solution with $h = 1/100$.*

fore this problem provides a severe test of our shock tracking algorithm, and especially tests our ability to handle small cells and wave interactions. Furthermore, since complex wave interactions occur after shock waves' collision, poor resolution will result near the interaction if the grid is not fine enough. For this reason we have used mesh refinement in addition to shock tracking in order to better resolve the solution.

For simplicity we assume that the tracked shocks do not cross the boundary between the coarse grid and the refined grid. The refinement boundary is thus in a region where the grid is regular and it is fairly straightforward to handle this interface using standard mesh refinement techniques (*e.g.*, Berger[2]). We will not discuss this further here. More details can be found in [27] and [36].

For this problem there is no mesh refinement initially. The mesh refinement is introduced after the shock waves' collision and used thereafter. The refinement region is chosen to contain all the tracked shocks within one fine grid with a buffer zone to prevent them from moving onto the coarse grid. For the results we present below, we take the coarse grid mesh size $h_c = 1/100$ as our underlying mesh size and use a mesh refinement ratio $m_r = 8$ for the fine grid, so that $h_f = 1/800$. The buffer zone has width $10h_c$, and a regridding step is done for every 16 time steps. Since the density jump is not prominent in this problem, we choose the max-norm of the jump in conserved quantities as our tracking criterion (with a tolerance $\varepsilon = 50$). Variable size time steps based on the fastest wave speed present and the uniform grid size $h_c$ or $h_f$ are used so that the Courant number is 0.9, ($m_r$ time steps are taken on the fine grid for each time step on the coarse grid.)

In Figure 8a, we show the density contour plot over both coarse and fine grids (density is plotted on a logarithmic scale). A blowup of the fine grid solution is shown in Figure 8b. Notice the fine wave structure following the interaction between the rightward going shock wave and the leftward going contact discontinuity. Without refinement, this wave pattern would not be clearly seen. Tracked points are shown in Figure 9.

To investigate the accuracy, we show plots of the density and velocity versus a finer grid ("true") solution, computed using $h_c = 1/800$ in the time before refinement is introduced, a)

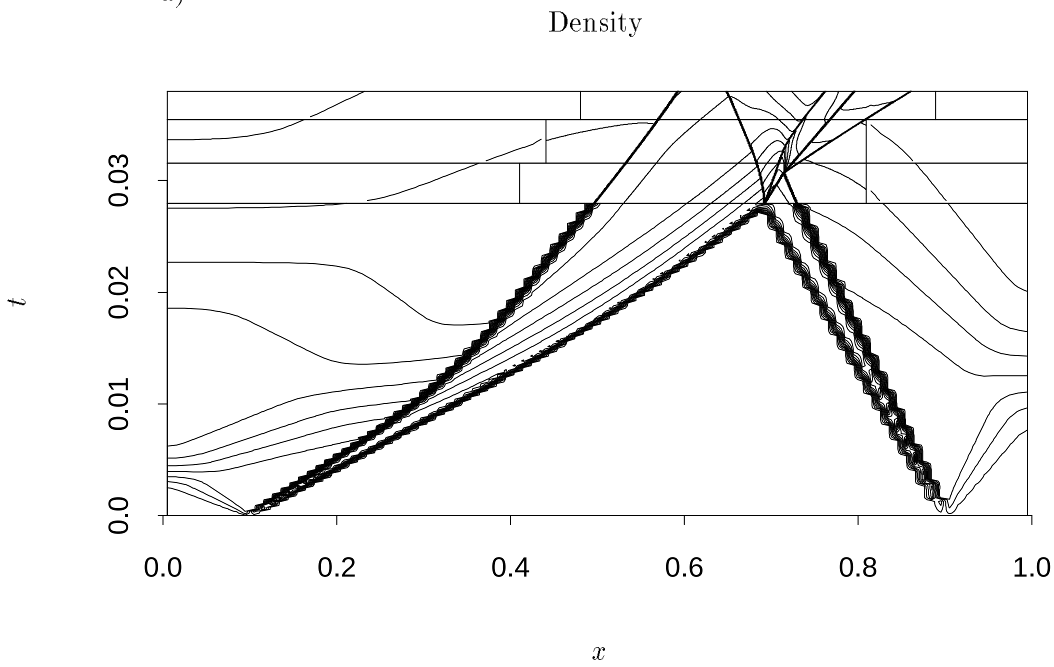


b)

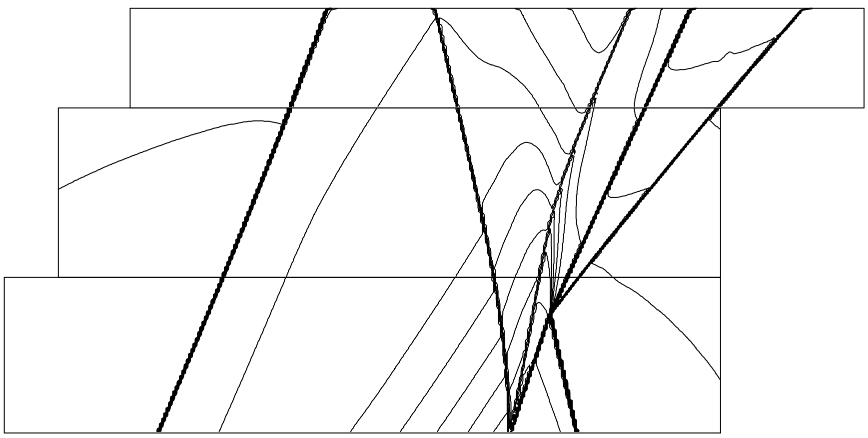

FIG. 8. *Density contour plots in the x-t plane (the contour lines are in the logarithmic scale) for the Woodward-Colella problem up to time $t = 0.038$ using the high resolution front tracking with adaptive mesh refinement algorithm with $h_c = 1/100$ and $m_r = 8$. a) Combined plot for both the coarse and fine grids. b) Blowup of the fine grid region.*

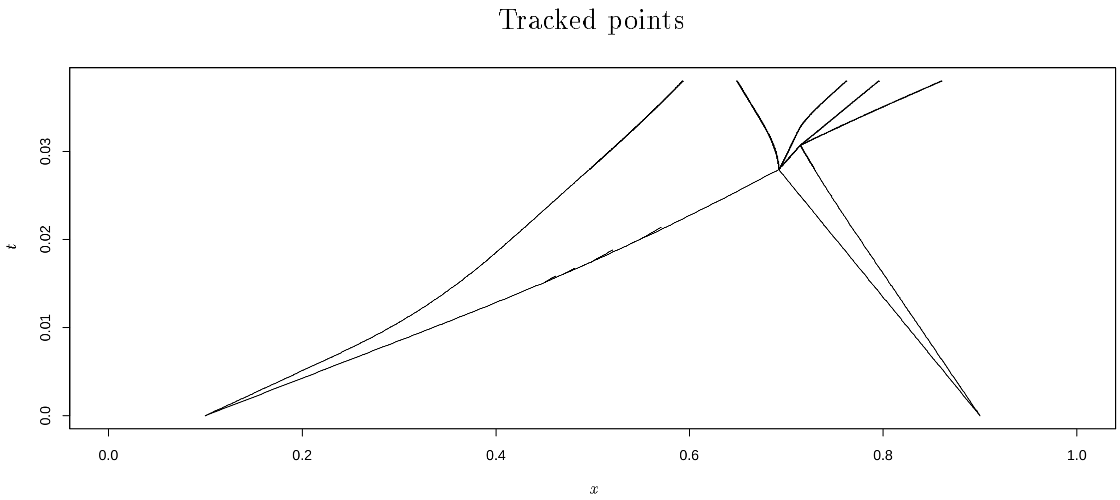


FIG. 9. *Tracked points for the Woodward-Colella problem.*

and then $h_c = 1/200$, $m_r = 8$ for refinement. Results at three different times are shown in Figure 10. Note that they are plotted using the most accurate cell values at each point. If a grid cell is in the fine grid region, we use the fine grid solution. Otherwise we use the coarse grid solution. We see good agreement between the two solutions. Notice the smooth transition between the coarse and fine grids. This indicates that our treatment of the coarse-fine grid interfaces is satisfactory.

As mentioned above, this is a difficult problem due to the very low pressure in the middle state. A rarefaction wave arising from the smooth flow behind the shock may move faster than the tracked shock, carrying a negative jump in pressure into the low pressure region that is of sufficient magnitude to result in a negative pressure. This is due to the linearization of the interaction between waves.

We currently deal with this problem by computing the interaction of the rarefaction wave with the strong shock wave exactly rather than using the wave linearization that is used elsewhere. We do this within the time step when the interaction occurs, modifying the strength and speed of these waves over the latter portion of the time step. This leads to some complication of the algorithm, but avoids the need to further restrict the time step and eliminates the difficulties (see [36] for more detail).

Naturally it would be preferable to find a more robust solution to this problem and work is continuing in this direction. We note, however, that this is a particularly difficult problem and that many production codes contain *ad hoc* procedures such as resetting negative pressures to positive values in order to deal with such problems. This is not a difficulty that arises solely from our shock tracking methodology. On the contrary, our approach has the advantage that it allows one to recognize these difficulties and deal with the interaction correctly and conservatively. (See [10] for an interesting discussion of this problem.)

**8. Unstable detonation waves.** As a more complex example that also includes stiff source terms modeling chemical reactions, we consider a model problem for combustion in which there are only two chemical species: "burnt gas" and "unburnt gas", and the

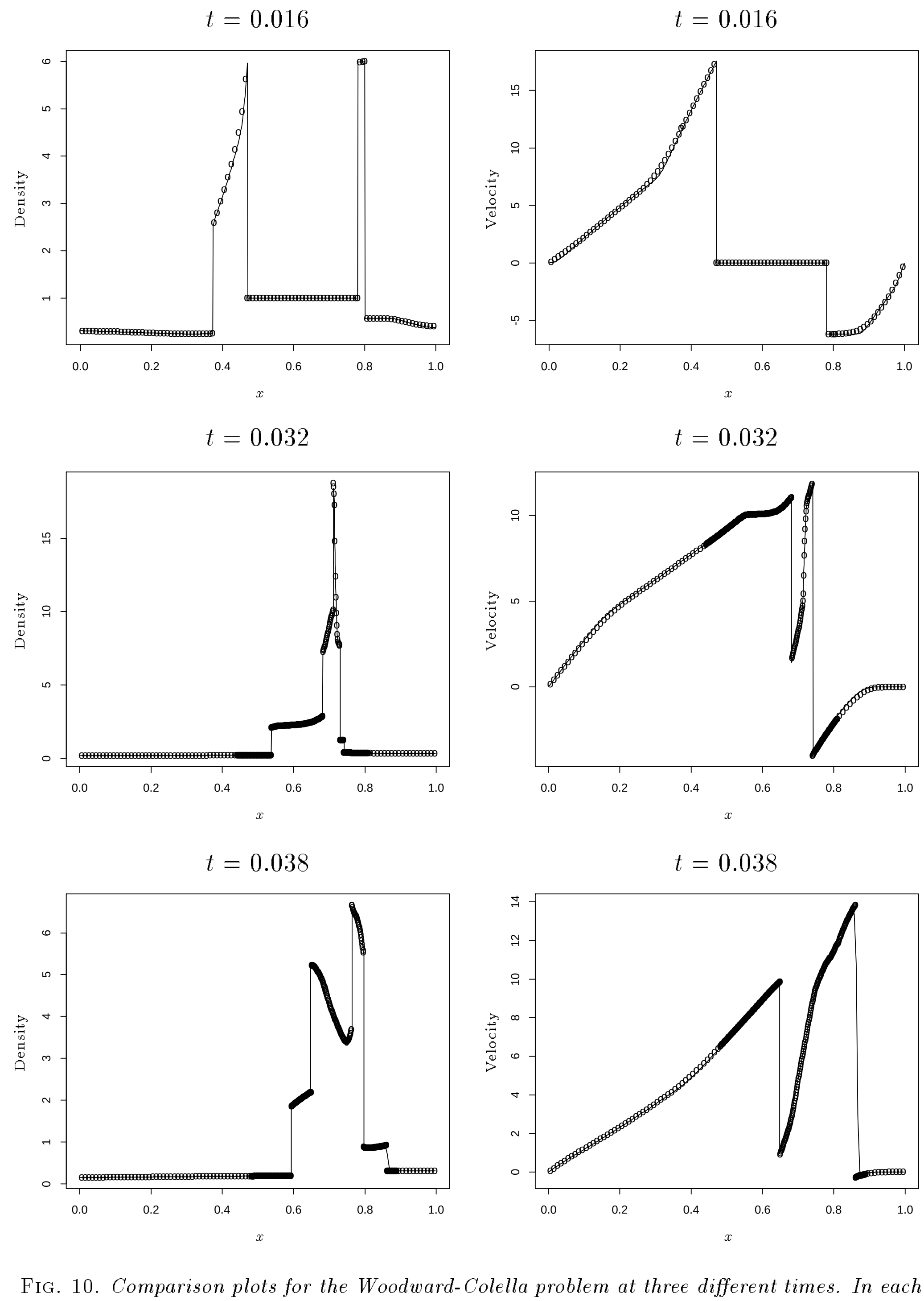


FIG. 10. *Comparison plots for the Woodward-Colella problem at three different times. In each figure, the solid line is the fine grid solution computed by $h_f = 1/800$ in the time when no refinement is used, and $h_c = 1/200$, $m_r = 8$ when the refinement is used. The points show the solution with $h_c = 1/100$ and $m_r = 8$. Density and velocity are shown.*

unburnt gas is converted to burnt gas *via* a simple decay process where the reaction rate $K(T)$ depends on the temperature. This model has been extensively studied in the past, e.g., [4], [6], [7], [8], [11].

Typically the reaction rate is very large when $T$ is sufficiently high but negligible for small $T$. For this combustion model, the Euler equations in one dimension take the form

$$\frac{\partial}{\partial t}\begin{pmatrix} \rho \\ \rho v \\ \rho E \\ \rho Z \end{pmatrix} + \frac{\partial}{\partial x}\begin{pmatrix} \rho v \\ \rho v^2 + p \\ (\rho E + p)v \\ \rho Z v \end{pmatrix} = -\begin{pmatrix} 0 \\ 0 \\ 0 \\ K(T)\rho Z \end{pmatrix} \tag{8.16}$$

where $Z$ is the mass fraction of the unburnt gas ($Z = 1$ for the unburnt gas and $Z = 0$ for the burnt gas). For simplicity we assume that both the unburnt gas and burnt gas are ideal gases with the same ratio of specific heats $\gamma$. Then by the ideal gas law, the temperature is given by $T = p/\rho R$ where $R$ is the universal gas constant. The equation of state is modified by the fact that the unburnt gas contains chemical energy that is released as heat in the process of burning. The total energy per unit mass takes the form

$$E = \frac{1}{\gamma - 1}p/\rho + \frac{1}{2}v^2 + q_0 Z \tag{8.17}$$

where $q_0$ is the heat release.

The reaction rate is given by the Arrhenius relation

$$K(T) = K_0 T^{\alpha} e^{-E^+/T} \tag{8.18}$$

where $K_0$ is the rate multiplier, $E^+$ is the activation energy, and $\alpha$ is the order of the reaction. We consider detonation wave solutions with the standard ZND structure (see, e.g., [8]) which consists of an ordinary fluid dynamic shock followed by a finite length chemical reaction zone.

A well-known difficulty in the detonation wave computation is that incorrect detonation wave speed can arise from numerical effects. This behavior is observed by Colella, Majda and Roytburd [6],[7] where a time-split method is used. They assert that if the chemistry is not fully resolved due to the insufficiently fine grids, incorrect detonation wave speeds will be obtained. Similar experiments have been reported in [23] and [28]. Another difficulty of modeling detonation waves is noticed by Bourlioux, Majda and Roytburd [4] in which classical one-dimensional stable and unstable detonation waves are tested. They conclude that false predictions of stability in the regime of physical instability as well as drastic predictions of instability for a physically stable detonation wave can be obtained with standard shock capturing methods if the grid is not sufficiently fine. In their paper, a shock tracking method with adaptive mesh refinement is proposed for the detonation wave computation, which combines the piecewise-parabolic method [46] with conservative front tracking [5] and adaptive mesh refinement [3]. They obtained very nice results which provides a basis for comparison for our shock tracking approach.

Let $s$ be a speed of the given ZND structure and $s_{CJ}$ the Chapman-Jouget speed. Then the parameter $f = (s/s_{CJ})^2$ measures the degree of overdrive of the detonation wave and satisfies $f \geq 1$. Now the problem of interest is to study the large time behavior of the overdriven detonation wave for a given ZND structure under small perturbation. It is known that the detonation wave is stable only if $f > f_{cr}$ where $f_{cr}$ is the critical value. For smaller $f$ the pressure just behind the shock wave is oscillatory and a train of oscillations is generated that propagates back from the reaction zone, as seen in the following figures. For comparison we choose a test case from [4], $f = 1.6$, in which the detonation is unstable. (The stable case $f = 1.8$ is also considered in [27].) Consequently other parameters are chosen the same as in [4], $\gamma = 1.2$, $R = 1$ (the universal gas constant), $\alpha = 0$, $q_0 = 50$, $E^+ = 50$. Throughout the tests, a steady ZND structure is used as the initial data with the unburnt state $\rho = 1$, $v = 0$, $p = 1$, $Z = 1$, and degree of overdrive $f$. Note that by specifying the unburnt state, $s_{CJ}$ can be calculated (see [41]). Then the speed of the ZND structure $s = s_{CJ}\sqrt{f}$ can be computed for a given $f$, so this ZND structure is uniquely defined. The destabilizing perturbation for each test is provided by the truncation error of the numerical method.

There are two characteristic length scales, the half reaction length $L_{1/2}$ and the half reaction time $t_{1/2}$, where $L_{1/2}$ is the distance required for half the mass fraction to be released in the ZND structure and $t_{1/2}$ is the time required for half the mass fraction to be released. These two values can be computed by evaluating the following integrals numerically:

$$L_{1/2} = -\int_{\frac{1}{2}}^{1} \frac{v\,dZ}{K(T)Z}, \tag{8.19}$$

$$t_{1/2} = -\int_{\frac{1}{2}}^{1} \frac{dZ}{K(T)Z}. \tag{8.20}$$

For the purpose of studying the grid effect on the numerical solutions, we normalize the length scale $x$ by choosing $K_0$ so that $L_{1/2} = 1$. We find that $K_0 = 231.16$ and $t_{1/2} = 0.891$ for $f = 1.6$.

We have used our shock tracking algorithm with only minor modification to solve this problem. A Strang splitting[38] is used to include the source terms, splitting between the homogeneous conservation laws and ordinary differential equations solved in each grid cell. Each time step consists of the following substeps:

1. Take a half time step by solving the ODEs in the old grid cells.
2. Take a full time step with the homogeneous equations using the shock tracking algorithm. This generates new grid cells.
3. Take a half time step again with the ODEs in the new grid cells after removing the old tracked points.

Here we solve the ODEs exactly with the frozen temperature to update the mass fraction $Z$.

Following [4] and [11], we monitor the shock front pressure, the pressure right behind the shock wave, as time evolves. This shock front pressure history will give a clear indication of the stability of a given ZND structure under small perturbation. Figure 11 shows the pressure behind the initiating shock as a function of time for three different choices of $f$ near the critical value $f_{cr} \approx 1.73$. We see that our algorithm correctly predicts stability or instability.

In order to investigate the grid effect on the numerical solution for this detonation wave problem, a convergence study for the shock front pressure history with three different coarse-fine grid spacings was performed with the following values of $h$:

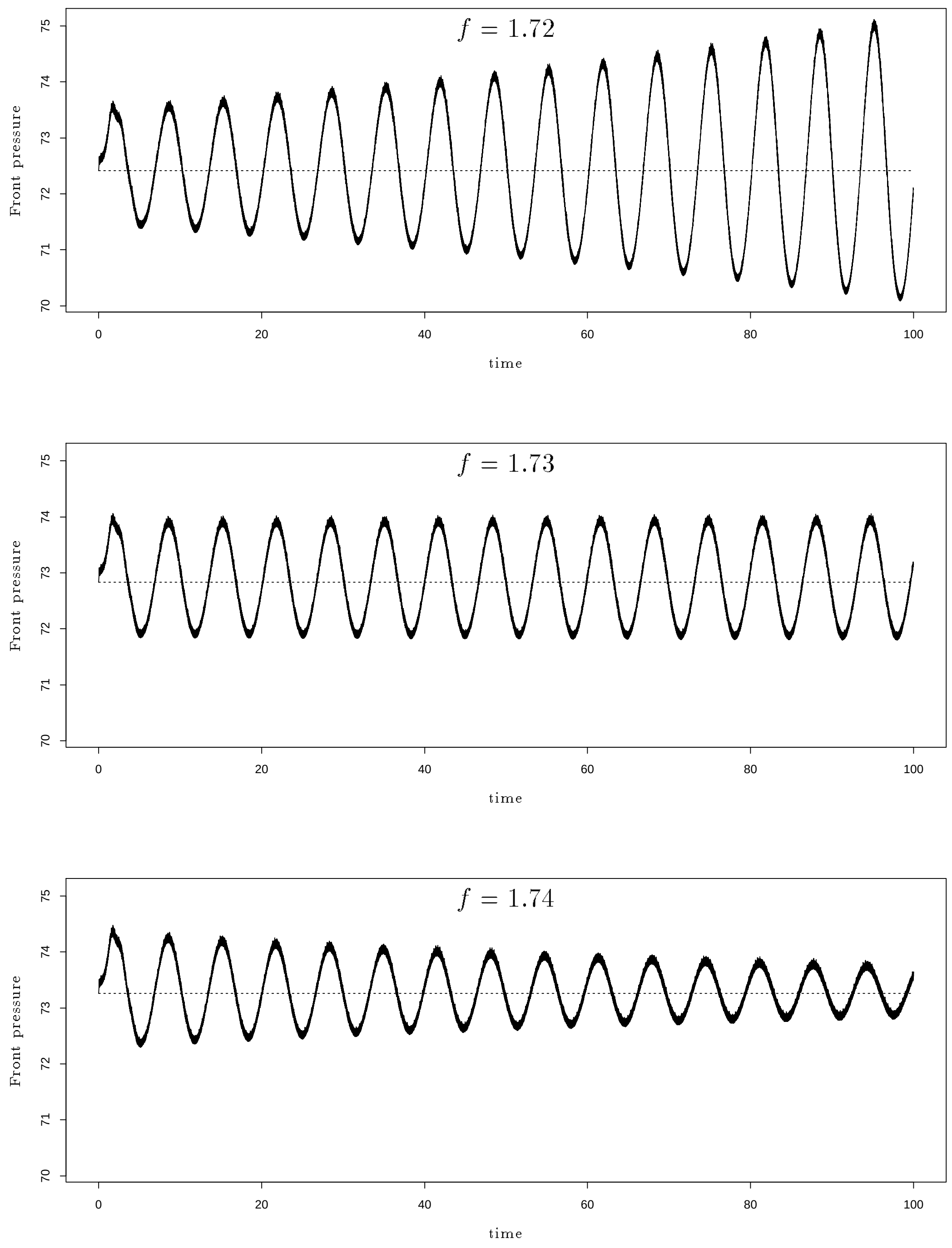


FIG. 11. *Shock front pressure history for values of the overdrive parameter $f$ near the critical value $f_{cr} \approx 1.73$. Theory and computations agree in predicting stability for larger values of $f$. The dashed line in each figure is the post-shock pressure in the steady ZND solution.*

1. coarse mesh $h_c = 1$ point $/L_{1/2}$, fine mesh $h_f = 4$ points$/L_{1/2}$,
2. coarse mesh $h_c = 2$ points$/L_{1/2}$, fine mesh $h_f = 8$ points$/L_{1/2}$,
3. coarse mesh $h_c = 4$ points$/L_{1/2}$, fine mesh $h_f = 16$ points$/L_{1/2}$.

Since there is only one tracked shock in this problem, the refinement region is chosen by going out a distance $20L_{1/2}$ on each side of the tracked shock. Courant number $\nu = 0.5$ is used for all the test cases. The tolerance $\varepsilon = 3$ for the jump in density is used for shock tracking.

Figure 12 shows results for the convergence study up to $t = 100$ in the computational domain $0 \le x \le 1000$. Our solution converges to a detonation wave with period $7.38 \pm 0.11$ (about $8.28t_{1/2}$) and peak pressure $99.83 \pm 0.2$. Note that the unperturbed shock front pressure for the unstable detonation is 67.36. The shock front pressure is magnified to a value nearly 50% higher than the initial value. Our solutions agree very well with values taken from the figures in [4].

To show the spatial resolution for the unstable detonation wave problem, we plot the pressure at three different times within one complete pressure front oscillation cycle as illustrated in Figure 12b, where the large dots indicate the plotting times. The results are shown in Figure 13. Note that an oscillatory wave structure appears behind the shock.

**9. Accuracy tests.** The results presented above give a strong indication that the shock tracking method developed here can accurately compute the solution to difficult problems. To give further evidence of the accuracy and convergence of our procedure, we now present some examples where the exact solution is known so that the error can be computed precisely and the order of accuracy estimated.

We first consider the linear advection equation

$$u_t + u_x = 0 \qquad \text{for} \quad 0 \le x \le 1 \tag{9.21}$$

with initial data

$$u(x,0) = \begin{cases} 2 + 1.5e^{20(x-0.32)} & x < 0.32 \\ 1 + 0.5\tanh(6\pi(0.36 - x)) & \text{otherwise.} \end{cases} \tag{9.22}$$

Our intention here is to study the accuracy achieved in cells near the discontinuity when the smooth solution is also rapidly varying, and in particular when there is an extreme point just behind the discontinuity. This is a challenging case that arises in some applications such as the detonation front in Section 8.

We have chosen the linear advection equation not only because the exact solution is easy to compute, but also because this is in some ways more difficult than a nonlinear problem. Errors made at one time step near a shock tend to have relatively little effect in future steps because the characteristics sweep information into the shock. In the linear problem where all characteristics are parallel, errors will accumulate and we would expect the peak in this problem to become badly smeared with most methods, see Figure 14.

Figure 15 shows results obtained with three different methods: shock capturing using the high resolution method of Section 3, shock tracking with this same method, and shock tracking with an improved estimate of the slopes using one-sided information near the tracked front as described at the end of Section 4. For each method the error is plotted as a function of time for 5 different grids with mesh sizes $h_l = 2^{1-l}/25$ and $k_l = h_l/2$ for

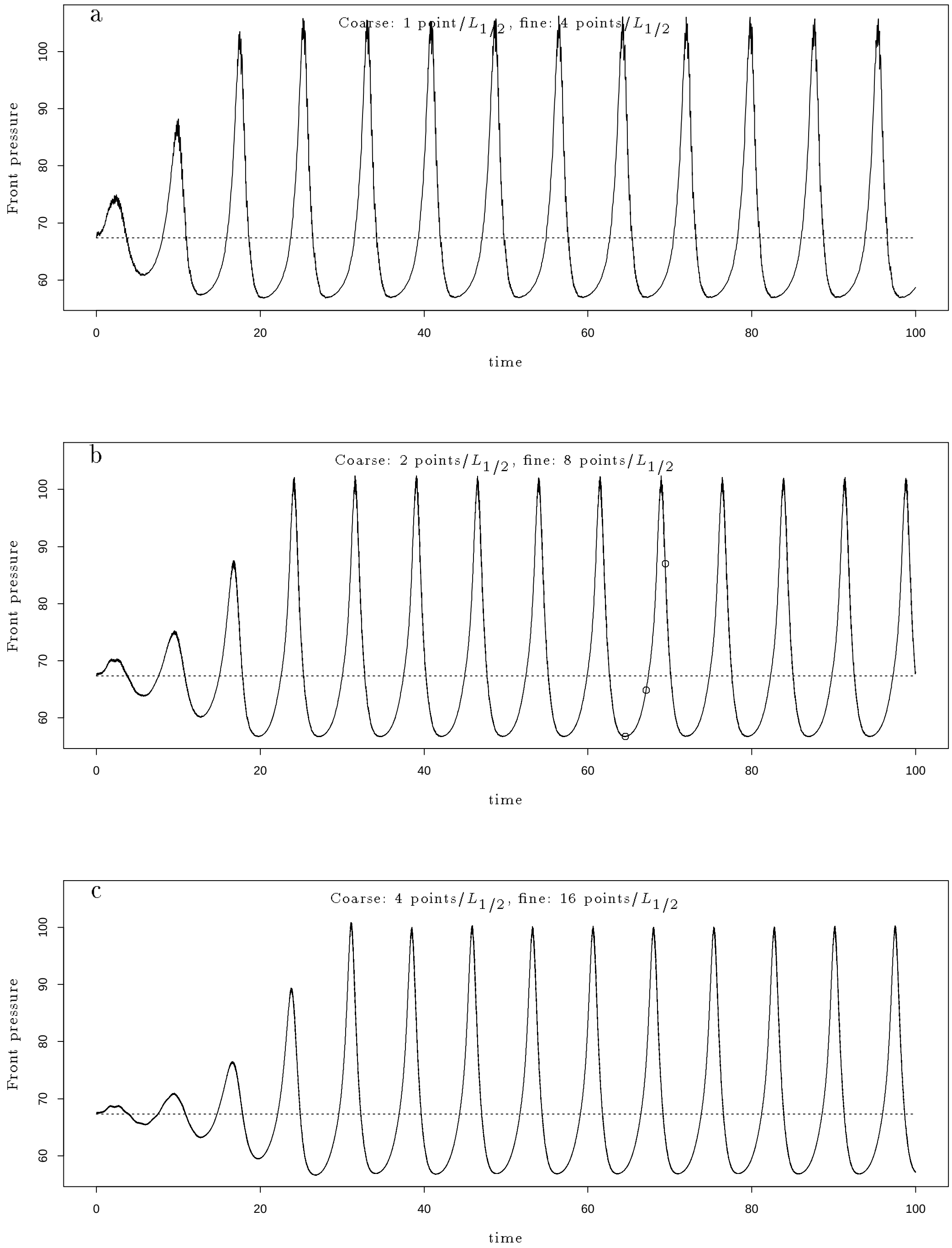


FIG. 12. *A convergence study for the shock front pressure history in an unstable detonation wave problem using high resolution shock tracking with adaptive mesh refinement. The dashed line in each figure is the post-shock pressure in the steady ZND solution.*

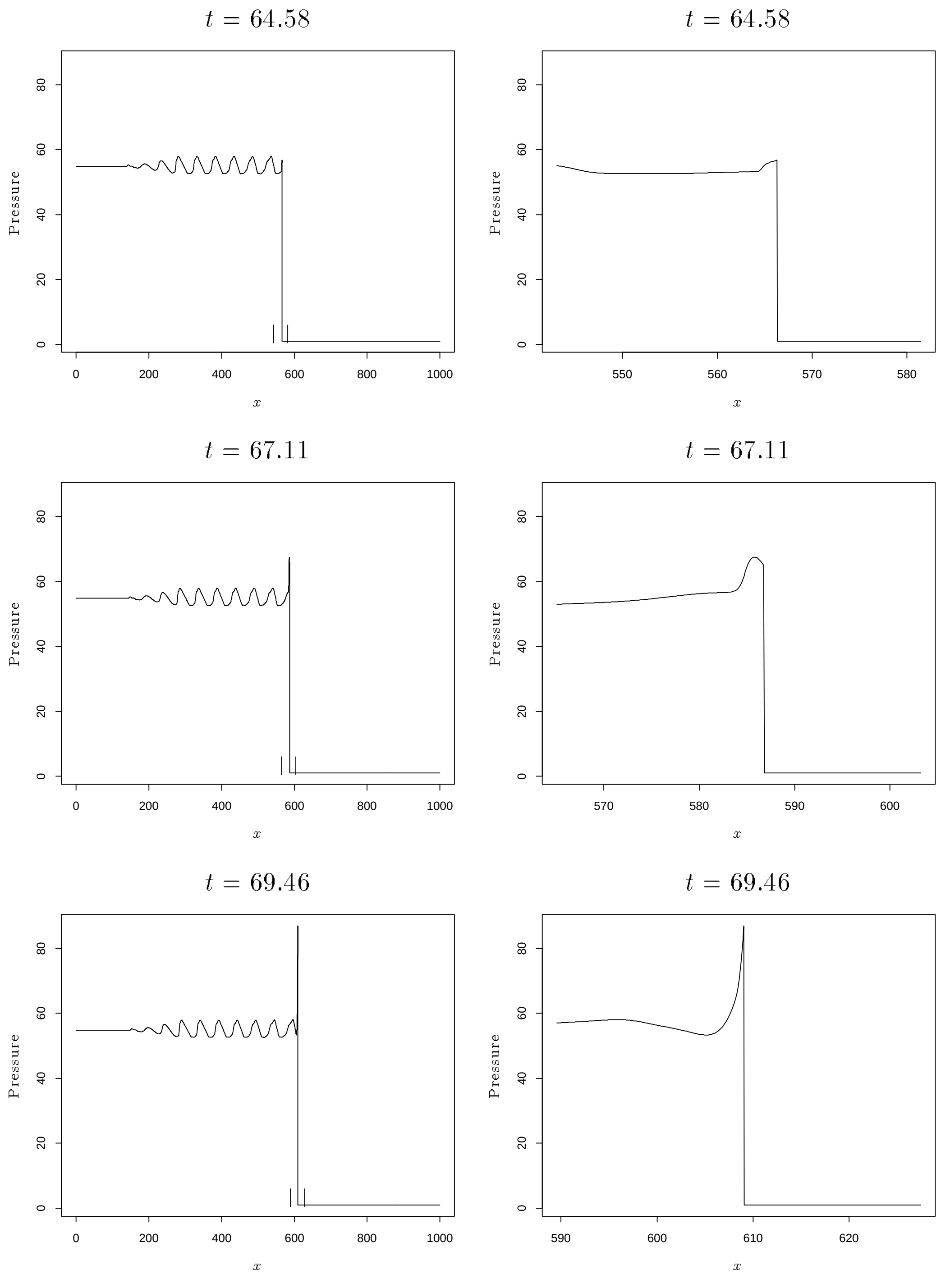


FIG. 13. *Spatial resolution for the unstable detonation problem at three different times as indicated by the dots in Figure 12b. The shock tracking method was used with mesh size $h_c = 2$ points/$L_{1/2}$, $h_f = 8$ points/$L_{1/2}$. The refined mesh is used only in the region indicated by the vertical bars near the x-axis around the tracked shock. The figures on the right are blowups of the refined grid solutions. Pressure is shown.*

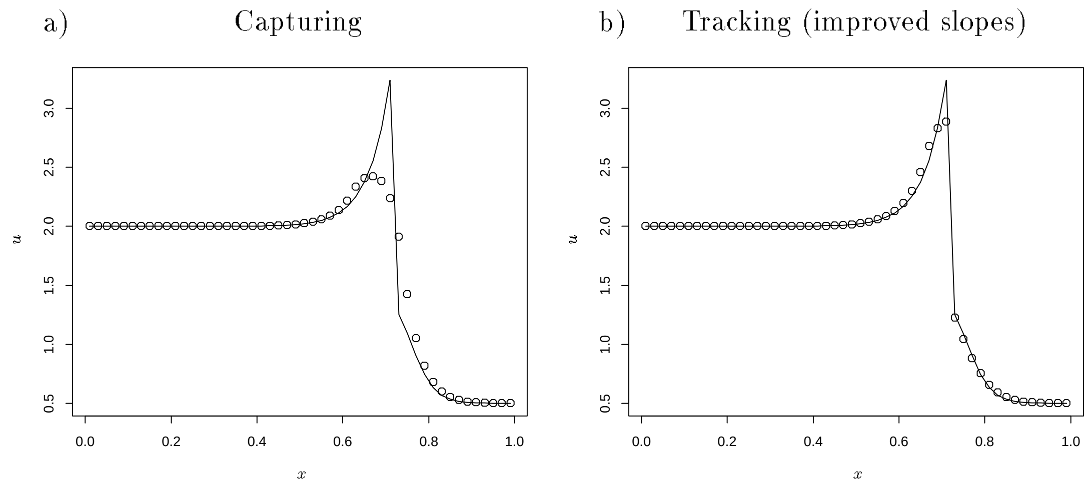


FIG. 14. *Numerical results for the linear advection equation (9.21) with data (9.22) at time* $t = 0.4$. *a) Result using the high resolution shock capturing method. b) Result using the high resolution shock tracking method with one-sided slopes. The solid line is the exact solution, and the points show the solution with* $h = 1/50$, $k = h/2$, *and the "minmod" limiter.*

$l = 1, 2, \cdots, 5$. The error is shown in both the 1-norm and the max-norm, and the order of accuracy is estimated at each time (in each norm) using the mesh refinement data.

We see that shock capturing gives no accuracy in the max-norm and roughly $O(\sqrt{h})$ convergence in the 1-norm as expected from the standard theory. The shock tracking method (with original slopes) gives roughly $O(h)$ accuracy in the 1-norm and convergence in the max-norm at rate $O(h^{0.2})$ or so. With improved slopes we get nearly $O(h)$ accuracy in the max-norm and somewhat better in the 1-norm. In these computations we have used the "minmod" slope limiter. Similar results are obtained with other limiters. Some comparisons are shown in [36].

As a second example we consider shock formation in Burgers' equation,

$$u_t + (u^2/2)_x = 0 \qquad \text{for} \quad -1 \le x \le 1 \tag{9.23}$$

with initial data

$$u(x, 0) = 1 + 0.5 \sin(\pi x), \tag{9.24}$$

and periodic boundary conditions. With these initial and boundary conditions, it is easy to show that the exact solution is smooth up to the shock formation time $t = 2/\pi \approx 0.64$, and is discontinuous afterward, see Whitham[44] for the detail on the construction of the exact solution.

Figure 16 shows results comparing shock capturing with shock tracking (improved slopes). With shock capturing we can clearly see the accuracy degrade markedly at the time of shock formation. With shock tracking there is some deterioration of accuracy near the shock formation time, but the accuracy then improves again as the tracked shock settles down to its correct location. Recall that we do not build into the algorithm any knowledge of the shock formation time or location. A discontinuity arising from one of the uniform cell interfaces starts to be tracked if its strength exceeds some value $\varepsilon$, which

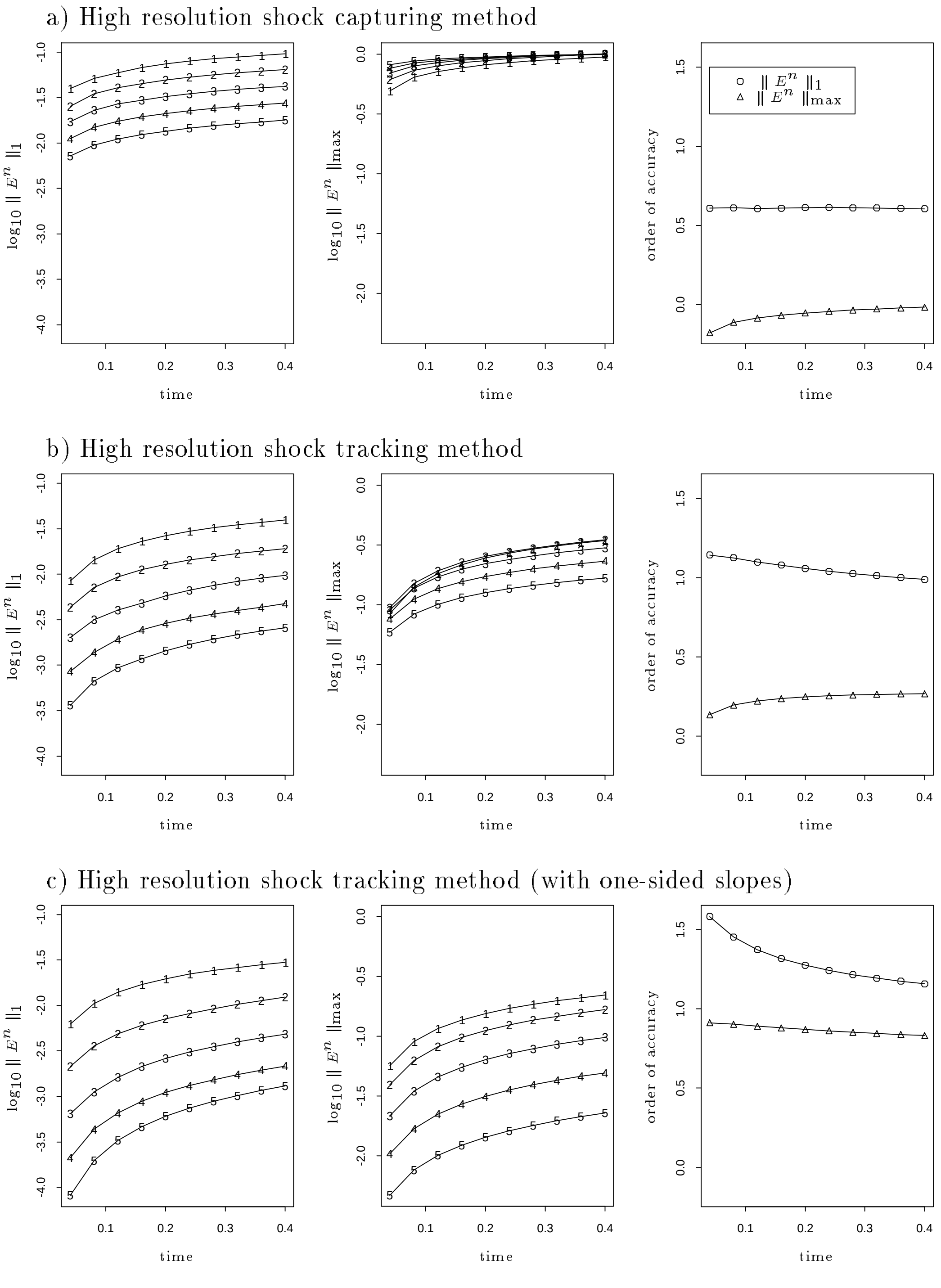


FIG. 15. *An accuracy study of three different methods for the linear advection equation (9.21) with initial data (9.22) up to time $t = 0.4$. Note that all the errors shown in the figure are plotted in the logarithmic scale with base 10. Error estimation is performed at 10 different times with a mesh refinement sequence $\{h_l = 2^{1-l}/25, l = 1, 2, \cdots, 5\}$. Results with the "minmod" slope limiter are shown.*

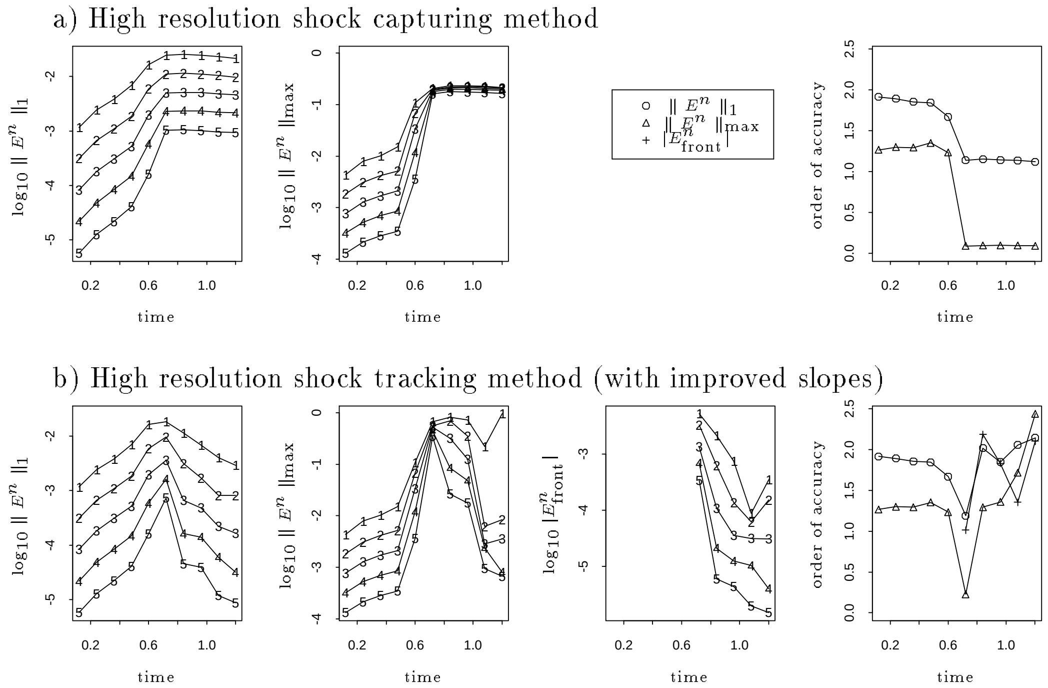


FIG. 16. *An accuracy study of the shock capturing and shock tracking methods for Burgers' equation (9.23) with initial data (9.24) up to time $t = 1.2$. Results with the "minmod" slope limiter are shown.*

was taken to be $\varepsilon = 0.35$ in these computations. We would not expect this to happen at exactly the correct time or location. In Figure 16, we have also shown the accuracy in the location of the tracked front relative to the exact shock location, and also the estimated order of accuracy of the front location. At least first order accuracy is seen at all times, with the magnitude of the error typically decreasing with time.

Finally, we show that reasonable convergence is still obtained on systems of equations. We consider the nonlinear isothermal equations

$$\frac{\partial}{\partial t}\begin{pmatrix} \rho \\ \rho v \end{pmatrix} + \frac{\partial}{\partial x}\begin{pmatrix} \rho v \\ \rho v^2 + c^2\rho \end{pmatrix} = 0 \tag{9.25}$$

where $c$ is the speed of sound, a constant here for which we take $c = 1$. The initial condition we use consists of a leftward going simple wave with velocity profile

$$v(x,0) = \tanh(6\pi(x - 0.64)) \qquad \text{for} \quad 0.4 \le x \le 1, \tag{9.26}$$

traveling from the left to right, and a rightward going Mach 2.89 shock wave at $x = 0.4$ traveling from the right to left. The density of the simple wave is computed from the Riemann invariant $R_+ = v + c\log(\rho)$, which is constant on the entire $\lambda_1 = v - c$ wave family, with $\rho_0 = 0.5$ and $v_0 = 0$ as the reference state (this determines the Riemann invariant constant). Note another Riemann invariant for this system is $R_- = v - c\log(\rho)$, which is constant on the $\lambda_2 = v + c$ family. Since these waves are approaching each other, wave interactions occur subsequently, see Figure 17a.

For this nonlinear wave interaction problem, due to the fact that there is no new wave family appearing after the head-on collision, we can compute the "exact" solution by

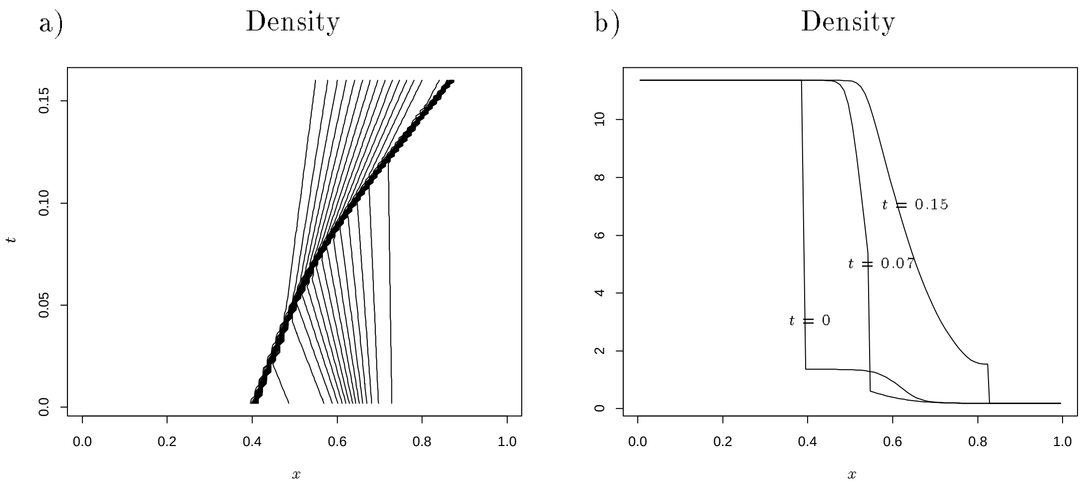


FIG. 17. *The exact solution for a wave interaction problem arising from the isothermal equations. a) Density contour plot in the $x$-$t$ plane (the contour lines are in the logarithmic scale). b) Snap shots of density at three different times.*

employing the Rankine-Hugoniot jump conditions at the shock together with the simple wave solutions on each side of the shock. Using this information would lead to a nonlinear ordinary differential equation for the shock location with respect to time. This can be solved numerically, using, for example, the ODE solver in the LSODE (Livermore Solver for Ordinary Differential Equations) Package. Once the shock location is known, the solution on both sides of the shock can be found using the method of characteristics. Figure 17b shows several snap shots of the exact solution.

Results for this problem using the shock capturing and shock tracking methods are shown in Figure 18 where the front error obtained from using the shock tracking method, the 1-norm error, and the max-norm error of the Riemann invariant $R_-$ are presented. It is very encouraging that our method produces results that converge at a fairly good rate in the 1-norm, despite the fact that the wave interaction of the strong and weak waves is handled linearly by allowing them to pass through each other without changing speed or magnitude.

**10. Conclusions.** We have presented a powerful shock tracking technique in one space dimension that is relatively easy to implement and capable of solving a variety of problems. There are four fundamental components to this algorithm:

1. The underlying grid is uniform.
2. Tracked points are moved according to the speeds that result from solving a Riemann problem. These points are used to define new grid cell boundaries, so that some uniform cells are subdivided.
3. A high resolution conservative method is used to update the solution on the resulting nonuniform grid. This method is defined in a very robust wave propagation form that allows arbitrarily small nonuniform cells relative to the time step.
4. When tracked waves collide, the time step is adjusted so that the collision is perfectly resolved by solving the Riemann problem at the beginning of the next time step.

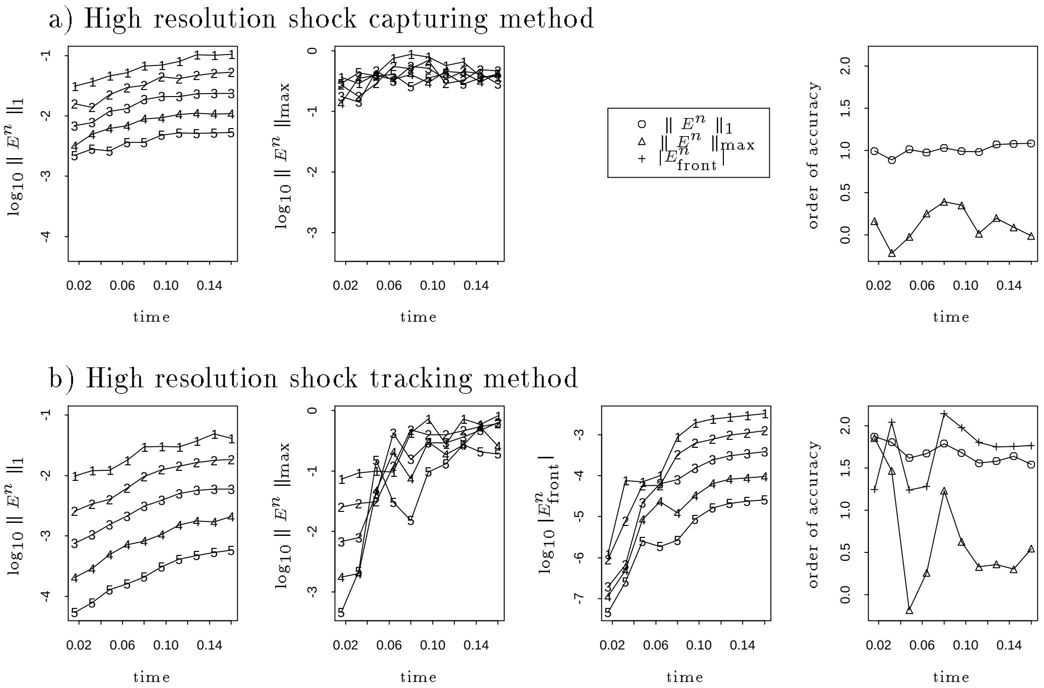


FIG. 18. *An accuracy study of the shock capturing and shock tracking methods for the isothermal equations (9.25) with initial data (9.26) up to time $t = 0.16$. Results for the Riemann invariant $R_-$ are shown.*

Shock formation, collisions, reflections from boundaries, and moving boundaries can all be handled in a uniform manner with minimal difficulty. Moreover, the tracking portion of this algorithm adds very little expense beyond that of high resolution shock capturing methods, since almost everywhere a method of this form is being used, on a uniform grid. It is only in the few grid cells that are directly affected by the front that a special treatment is needed.

The basic philosophy behind our approach is that the front location need not be exactly correct, since a conservative method is used on the resulting grid, but that by introducing interfaces in approximately the correct location it is possible to resolve discontinuities far better than would be possible on a uniform grid, with modest additional cost. The results in this paper show that this works extremely well in one space dimension.

This also turns out to be surprisingly effective in two dimensions. The first three components can be extended quite naturally to more space dimensions. Again a uniform underlying grid can be used with some grid cells subdivided by a piecewise linear front. The front can be moved by solving Riemann problems normal to the front and the resulting wave structure used to choose a new front location. Naturally this is more complicated in two dimensions than in one, but at least for the case of a single front this can be done fairly easily in an effective manner. A conservative high resolution wave propagation method[21, 25] is then used on the resulting nonuniform grid to update the solution. A two-dimensional front tracking algorithm has been developed by the second author[36] using this approach and has been successfully used both for shock propagation and fluid interface problems. Some preliminary results for a porous media multiphase flow problem and a Rayleigh-Taylor unstable interface are given in [37]. A paper describing the two-dimensional shock tracking in more detail is currently in preparation[26].

**Acknowledgements.** This work was supported in part by NSF Grants DMS-8657319, DMS-9204329 and was conducted while the second author was a graduate student in the Applied Mathematics Department at the University of Washington. This work was also supported by ETH-Zürich and the authors would like to thank ETH and particularly the members of the Seminar für Angewandte Mathematik for their hospitality and support.

## REFERENCES

[1] A. V. Aho, J. E. Hopcroft, and J. D. Ullman, *Data Structures and Algorithms*, Addison-Wesley, 1987.

[2] M. J. Berger, *On conservation at grid interfaces*, SIAM J. Numer. Anal., 24 (1987), pp. 967–984.

[3] M. J. Berger and P. Colella, *Local adaptive mesh refinement for shock hydrodynamics*, J. Comput. Phys., 82 (1989), pp. 64–84.

[4] A. Bourlioux, A. J. Majda, and V. Roytburd, *Theoretical and numerical structure for unstable one-dimensional detonations*, SIAM J. Appl. Math., 51 (1991), pp. 303–343.

[5] I.-L. Chern and P. Colella, *A conservative front tracking method for hyperbolic systems of conservation laws*, UCRL-97200, LLNL, (1987).

[6] P. Colella, A. Majda, and V. Roytburd, *Fractional step methods for reacting shock waves*, in Lectures in Applied Mathematics, vol 24, American Mathematical Society, 1986, pp. 459–477.

[7] ———, *Theoretical and numerical structure for reacting shock waves*, SIAM J. Sci. Stat. Comput., 7 (1986), pp. 1059–1080.

[8] R. Courant and K. O. Friedrichs, *Supersonic Flow and Shock waves*, McGraw-Hill, New York, 1954.

[9] C. M. Dafermos, *Polygonal approximation of solution to the initial value problem for a conservation law*, J. Math. Anal. Appl., 38 (1972), pp. 33–41.

[10] B. Einfeldt, C. D. Munz, P. L. Roe, and B. Sjogreen, *On Godunov type methods near low densities*, J. Comput. Phys., 92 (1991), pp. 273–295.

[11] W. Fickett and W. W. Wood, *Flow calculations for pulsating one-dimensional detonations*, Phys. Fluids, 9 (1966), pp. 903–916.

[12] B. A. Finlayson, *Numerical Methods for Problems with Moving Fronts*, Ravenna Park Publishing Inc., 1992.

[13] A. Harten, *ENO schemes with subcell resolution*, J. Comput. Phys., 83 (1989), pp. 148–184.

[14] A. Harten and J. M. Hyman, *Self-adjusting grid methods for one-dimensional hyperbolic conservation laws*, J. Comput. Phys., 50 (1983), pp. 235–269.

[15] G. W. Hedstrom, *Some numerical experiments with Dafermos's method for nonlinear hyperbolic equations*, in Lecture notes in Mathematics, Vol. 267, Springer, Berlin, 1972.

[16] J. M. Hyman, *Numerical methods for tracking interfaces*, Physica D, 12 (1984), pp. 396–407.

[17] D. E. Knuth, *The Art of Computer Programming*, vol. 1, Addison-Wesley, 2 ed., 1973.

[18] R. J. LeVeque, *Convergence of a large time step generalization of Godunov's method for conservation laws*, Comm. Pure Appl. Math., 37 (1984), pp. 463–477.

[19] ———, *A large time step generalization of Godunov's method for systems of conservation laws*, SIAM J. Numer. Anal., 22 (1985), pp. 1051–1073.

[20] ———, *Shock-tracking with the large time step method*, in Proc. 7th Intl. Conf. Comput. Meth. in Appl. Sci. Eng., R. Glowinski and J.-L. Lions, eds., Versailles,France, 1985.

[21] ———, *High resolution finite volume methods on arbitrary grids via wave propagation*, J. Comput. Phys., 78 (1988), pp. 36–63.

[22] ———, *Second order accuracy of Brenier's time-discrete method for nonlinear system of conservation laws*, SIAM J. Numer. Anal., 25 (1988), pp. 1–7.

[23] ———, *Hyperbolic conservation laws and numerical methods*, in Von Karman Institute for Fluid Dynamics, 1990. Lecture series on computational fluid dynamics 1990-03.

[24] ———, *Numerical Methods for Conservation Laws*, Birkhäuser-Verlag, 1990.

[25] ———, *Simplified multi-dimensional flux limiter methods*, in Proc. ICFD Conf. Numer. Meth. for Fluid Dyn., Reading, 1992.

[26] R. J. LeVeque and K.-M. Shyue, *Two-dimensional front tracking based on high resolution wave propagation methods*. in preparation.

[27] ———, *Shock tracking based on high resolution wave propagation methods*, Technical report No. 92-3, Department of Applied Mathematics, University of Washington, (1992).

[28] R. J. LeVeque and H. C. Yee, *A study of numerical methods for hyperbolic conservation laws with stiff source terms*, J. Comput. Phys., 86 (1990), pp. 187–210.

[29] D.-K. Mao, *A treatment of discontinuities in shock-capturing finite difference methods*, J. Comput. Phys., 92 (1991), pp. 422–455.

[30] ———, *A treatment of discontinuities for finite difference methods in the two dimensional case*, J. Comput. Phys., 104 (1993), pp. 377–397.

[31] W. F. Noh, *A time-dependent, two-space-dimensional coupled Eulerian-Lagrangian code*, Methods in Comput. Phys., (1964).

[32] E. S. Oran and J. P. Boris, *Numerical Simulation of Reactive Flow*, Elsevier, New York, 1987.

[33] N. H. Risebro and A. Tveito, *Front tracking applied to a nonstrictly hyperbolic system of conservation laws*, SIAM J. Sci. Stat. Comput., 12 (1991), pp. 1401–1419.

[34] ———, *A front tracking method for conservation laws in one dimension*, J. Comput. Phys., 101 (1992), pp. 130–139.

[35] P. L. Roe, *Approximate Riemann solvers, parameter vector, and difference scheme*, J. Comput. Phys., 43 (1981), pp. 357–372.

[36] K.-M. Shyue, *Front Tracking Methods based on Wave Propagation*, Ph.D. thesis, University of Washington, June, 1993.

[37] ———, *Front tracking based on high-resolution wave propagation methods*, Proc. Symp. Appl. Math., (to appear).

[38] G. Strang, *On the construction and comparison of difference schemes*, SIAM J. Numer. Anal., 5 (1968), pp. 506–517.

[39] B. K. Swartz and B. Wendroff, *AZTEC: a front tracking code based on Godunov's method*, Appl. Numer. Math., 2 (1986), pp. 385–397.

[40] P. K. Sweby, *High resolution schemes using flux limiters for hyperbolic conservation laws*, SIAM J. Numer Anal., 21 (1984), pp. 995–1011.

[41] Z.-H. Teng, A. J. Chorin, and T.-P. Liu, *The Riemann problem for reacting gas, with applications to transition*, SIAM J. Appl. Math., 42 (1982), pp. 964–981.

[42] B. van Leer, *Towards the ultimate conservative difference scheme V. A second order sequel to Godunov's method*, J. Comput. Phys., 32 (1979), pp. 101–136.

[43] B. Wendroff, *An analysis of front tracking for chromatography*, preprint, (1991).

[44] G. B. Whitham, *Linear and Nonlinear Waves*, John Wiley & Sons, Inc., New York, 1974.

[45] P. Woodward and P. Colella, *The numerical simulation of two-dimensional fluid flow with strong shock*, J. Comput. Phys., 54 (1984), pp. 115–173.

[46] ———, *The piece-wise parabolic method (PPM) for gas dynamical simulations*, J. Comput. Phys., 54 (1984), pp. 174–201.